

**LINEAR DEMULTIPLE SOLUTION BASED ON BOTTOM-MULTIPLE  
GENERATOR (BMG) REFLECTOR APPROXIMATION: SUBSALT EXAMPLE**

A Thesis

by

ABIOLA OMOBOLAJI OLADEINDE

Submitted to the Office of Graduate Studies of  
Texas A&M University  
in partial fulfillment of the requirements for the degree of

MASTER OF SCIENCE

August 2005

Major Subject: Geophysics

**LINEAR DEMULTIPLE SOLUTION BASED ON BOTTOM-MULTIPLE  
GENERATOR (BMG) REFLECTOR APPROXIMATION: SUBSALT EXAMPLE**

A Thesis

by

ABIOLA OMOBOLAJI OLADEINDE

Submitted to the Office of Graduate Studies of  
Texas A&M University  
in partial fulfillment of the requirements for the degree of

MASTER OF SCIENCE

Approved by:

Chair of Committee,  
Committee Members,  
Head of Department,

Luc T. Ikelle  
Hongbin Zhan  
Daulat D. Mamora  
Richard L. Carlson

August 2005

Major Subject: Geophysics

**ABSTRACT**

Linear Demultiple Solution Based on  
Bottom-Multiple Generator (BMG) Reflector Approximation:

Subsalt Example. (August 2005)

Abiola Omobolaji Oladeinde,

B.S., University of Ibadan, Nigeria

Chair of Advisory Committee: Dr. Luc T. Ikelle

Significant quantities of hydrocarbons are found in complex salt environments. One of the modern challenges of exploration and production activities is to image below salt. This challenge arises from the complexities of salt structures, weak primaries from the subsalt, and the interference of free-surface multiples with the weak primaries of the subsalt. To effectively process subsalt data, we need to develop a method of attenuating free-surface multiples that preserves the amplitude and phase of primaries and does not introduce artifacts at either near and far offsets. In this thesis, we will demonstrate that the weak primaries of the subsalt can be preserved while attenuating free-surface multiples. The method used for the demonstration is the bottom-multiple generator (BMG) reflector approximation. This technique requires that a portion of the data containing only primaries be defined. A multidimensional convolution of the data containing only primaries with the actual data will predict free-surface multiples and hence is used to attenuate free-surface multiples from the actual data. This method is one of the most effective methods for attenuating free-surface multiples; however, the

method requires muting data at the BMG location. One of the issues investigated in this thesis, is to establish the sensitivity of the BMG demultiple technique when the mute at the BMG location end up cutting some seismic reflections, which can be the case in complex environments such as the Gulf of Mexico and Gulf of Guinea, where free-surface multiples interfere with primaries. For this investigation, we generated synthetic data through the 2D elastic finite-difference modeling technique. The synthetic seismic data contain primaries; free-surface multiples, and internal multiples, and direct waves acquired over a 2D geological model that depicts a shallow-water geology.

In this thesis, we also investigate if the first step of the BMG demultiple technique can sufficiently attenuate free-surface multiples. For this investigation, we designed a 2D geological model, which depicts the deep offshore environment, and we generated synthetic data through the 2D elastic finite-difference modeling technique.

After performing the various investigations mentioned above, the following conclusions were made, that the demultiple result is not affected when the mute at the BMG location end up cutting some primaries, that the first step of the BMG demultiple technique is not sufficient for the demultiple, and that the weak subsalt primaries are preserved during demultiple processes. We compared shot gathers and zero offset data before and after the demultiple.

## **DEDICATION**

To my husband, my wonderful gift from God.

## ACKNOWLEDGMENTS

My sincere appreciation goes to my academic advisor, Dr. Luc Ikelle for his teaching, his support financial and morally. His supports have played a great role in the completion of this program and have been fundamental to my growth as a geophysicist.

I would also like to express my gratitude to my committee members, Dr. Hongbin Zhan and Dr. Daulat Mamora, for their comments and valuable time.

My appreciation also goes to former and current CASP members, who provided technical support and fond memories, as well as all the sponsors of the CASP project that made this and other research possible.

I would probably not be writing this if it were not for the unconditional support of my family. They taught me and showed me the value of unity and love. Along with my family I thank my friends who enrich my life day by day.

Finally and above all, I thank my God, whose grace is sufficient for me.

## TABLE OF CONTENTS

		Page
ABSTRACT .....		iii
DEDICATION .....		v
ACKNOWLEDGMENTS.....		vi
TABLE OF CONTENTS .....		vii
LIST OF FIGURES.....		ix
LIST OF TABLES .....		x
CHAPTER		
I	INTRODUCTION.....	1
	Problem Description.....	6
	Multiples.....	6
	Internal Multiples .....	6
	Free-surface Multiples .....	7
	A Review of Demultiple Techniques .....	9
	Demultiple Technique Based on Periodicity.....	10
	Predictive Deconvolution.....	10
	Demultiple Technique Based on Separability .....	11
	CMP Stacking .....	11
	F-K Filter.....	12
	Radon Transform .....	14
	Demultiple Technique Based on Prediction and Subtraction .....	14
	Inverse Scattering Multiple Attenuation (ISMA) .....	14
	Summary .....	15
II	A BRIEF BACKGROUND ON CONSTRUCTING FREE- SURFACE MULTIPLES.....	16
	Prediction of Free-Surface Multiples .....	16

CHAPTER	Page
III	CONCEPTS OF BOTTOM-MULTIPLE GENERATOR (BMG) REFLECTOR APPROXIMATION..... 20
	Subtraction of Predicted Free-Surface Multiples ..... 20
	Review on Bottom-Multiple Generator (BMG) Reflector Approximation..... 25
	How to Obtain Particle Velocity from Pressure Data ..... 30
	Potential Errors..... 31
	Conclusions ..... 33
	Novelty and Importance of the BMG Demultiple Technique ..... 33
IV	ANALYSIS OF THE EFFECT OF BOTTOM-MULTIPLE GENERATOR (BMG) APPROXIMATION IN COMPLEX GEOLOGY ..... 34
	Geological Models Description..... 34
	Application of the BMG Demultiple Technique..... 37
	Case I: Shallow-Water Geology..... 37
	Case II: Deep-Water Geology ..... 48
V	SUMMARY AND CONCLUSIONS..... 63
	REFERENCES..... 65
	APPENDIX A ..... 67
	APPENDIX B ..... 81
	VITA ..... 87



**LIST OF TABLES**

TABLE		Page
4.1	Modeling parameters of the subsurface layers in Figure	
	4.1 .....	35
4.2	Modeling parameters of the subsurface layers in Figure	
	4.2 .....	36

## LIST OF FIGURES

FIGURE		Page
1.1	An illustration of ray paths common to various seismic events in towed-streamer data .....	2
1.2	The complex 2D geological models (adapted from Lafond et al. 2004) considered for our investigations. The models consist of two isolated salt bodies, which lie close to the seafloor. (a) Shallow-water geology. Layers 5, 6, 7, and 8 are the subsalt layers. (b) Deep-water geology. Layers 4, 5, 6, and 7 are the subsalt layers .....	4
1.3	Zero offset data before demultiple. (a) Shallow-water geology. (b) Deep-water geology .....	5
1.4	An illustration of different types of internal multiples common to marine acquisition .....	7
1.5	An illustration of different types of free-surface multiples common to marine acquisition. ....	8
1.6	An example of f-k filtering for free-surface multiple attenuation (Ikelle and Amundsen, 2003) .....	13
2.1	An illustration of possible ways in which seismic events can be constructed for towed-streamer data .....	17
2.2	An illustration of possible ways in which free-surface multiples can be constructed for towed streamer data .....	19

FIGURE	Page
3.1	An illustration of the crosscorrelation of the actual data containing primaries and free-surface multiples with the predicted free-surface multiples. Notes that we are interested in the crosscorrelation of free-surface multiples in the actual data with the predicted free-surface multiples ..... 24
3.2	An illustration of the autocorrelation of the predicted free-surface multiples ..... 24
3.3	The dotted line represents the BMG reflector ..... 25
3.4	An illustration of predicted free-surface multiples obtained from the multidimensional convolution of $V_0^a$ with $\Phi_0$ . Note that only free-surface multiples that have their first bounce in the subsurface located above the BMG reflector is predicted and hence attenuated from the actual data, $\Phi_0$ ..... 27
3.5	An illustration on how the BMG reflector can be define from the autoconvolution of the data ..... 28
3.6	An illustration of free-surface multiples predicted from the multidimensional convolution of $V_{pa}^b$ with $\Phi_0^a$ ..... 29
3.7	An illustration of free-surface multiples not predicted in the two steps of the BMG demultiple technique. Note that these types of free-surface multiples are usually weak in deep-water and are hardly visible ..... 30

FIGURE	Page
4.1	Complex 2D shallow-water geology (adapted from Lafond et al. 2004) considered for our investigation of the BMG demultiple technique (Case I). Layers 5, 6, 7, and 8 are the subsalt layers ..... 35
4.2	Complex 2D deep-water geology (adapted from Lafond et al. 2004) considered for our investigation of the BMG demultiple technique (Case II). Layers 4, 5, 6, and 7 are the subsalt layers ..... 36
4.3	Shot gather of the shot located at 500 m considered for our analysis ..... 40
4.4	An example of data containing only primaries located above the BMG reflector ..... 40
4.5	An example of the field of predicted free-surface multiples obtained from the multidimensional convolution of $V_0^a$ with $\Phi_0$ ..... 41
4.6	The first demultiple result obtained after the application of the first step of the demultiple technique ..... 41
4.7	An example of the data located below the BMG reflector ..... 42
4.8	An example of the field of predicted free-surface multiples obtained from the multidimensional convolution of $V_{pa}^b$ with $\Phi_0^a$ ..... 42

FIGURE	Page
4.9	An example of the actual data from shot located at 500 m ..... 43
4.10	An example of the final demultiple result after the application of the second step of the BMG demultiple technique ..... 43
4.11	Zero offset data of the actual data before demultiple ..... 45
4.12	Zero offset data of the first demultiple result. .... 46
4.13	Zero offset data of the final demultiple result ..... 47
4.14	Shot gather of shot located at 500 m considered for the deep- water geology ..... 50
4.15	An example of the data containing only primaries located above the BMG reflector ..... 50
4.16	An example of the field of predicted free-surface multiples obtained from the multidimensional convolution of $V_0^a$ with $\Phi_0$ ..... 51
4.17	An example of the first demultiple result..... 51
4.18	An example of the portion of data located below the BMG reflector ..... 52

FIGURE	Page
4.19	Shot gather showing the field of predicted free-surface multiples obtained from the multidimensional convolution of $V_{pa}^b$ with $\Phi_0^a$ ..... 52
4.20	(a) An example of shot gather from the actual data (shot located at 500 m) before demultiple. (b) The first demultiple result (c) The second demultiple result ..... 53
4.21	Shot gather of shot located at 3000 m considered for our analysis ..... 55
4.22	An example of the portion of the data containing only primaries located above the BMG reflector ..... 55
4.23	The field of predicted free-surface multiples obtained from the multidimensional convolution of $V_0^a$ with $\Phi_0$ ..... 56
4.24	An example of the first demultiple result ..... 56
4.25	This is an example of the portion of $\Phi_{pa}$ located below the BMG reflector ..... 57
4.26	Shot gather showing an example of the field of predicted free-surface multiples obtained from multidimensional convolution of $V_{pa}^b$ with $\Phi_0^a$ ..... 57

FIGURE	Page
4.27 (a) An example of shot gather from the actual data (shot located at 3000 m) before demultiple (b) The first demultiple result (c) The second demultiple result .....	58
4.28 Zero offset of the synthetic towed-streamer data (deep-water geology) before demultiple .....	60
4.29 Zero offset of the synthetic towed-streamer data obtained after the first demultiple step .....	61
4.30 Zero offset of the synthetic towed-streamer data obtained after the second demultiple step .....	62

## CHAPTER I

### INTRODUCTION

The common seismic events recorded during marine acquisition (for example towed-streamer data) are direct waves, primaries, free-surface multiples, internal multiples, and ghosts of both source and receivers. (Figure 1.1 shows an illustration of typical ray paths describing the seismic events in towed-streamer data). The challenges faced in towed-streamer data processing are to attenuate free-surface multiples and imaging primaries. Note that internal multiples are weak compare to the primaries and are therefore considered negligible. Note also that the ghosts of sources and receivers are treated as part of the multiple attenuation.

In this thesis, we focus on attenuating free-surface multiples in towed-streamer data. Several demultiple techniques have been developed and new techniques are being proposed. Most of the demultiple techniques have underlying assumptions. It is important that the assumptions are taken into account when applying the demultiple techniques. Some demultiple techniques introduce artifacts to the data or fail in complex environments, such as the subsalt and sub-basalt.

---

This thesis follows the style and format of Geophysics.



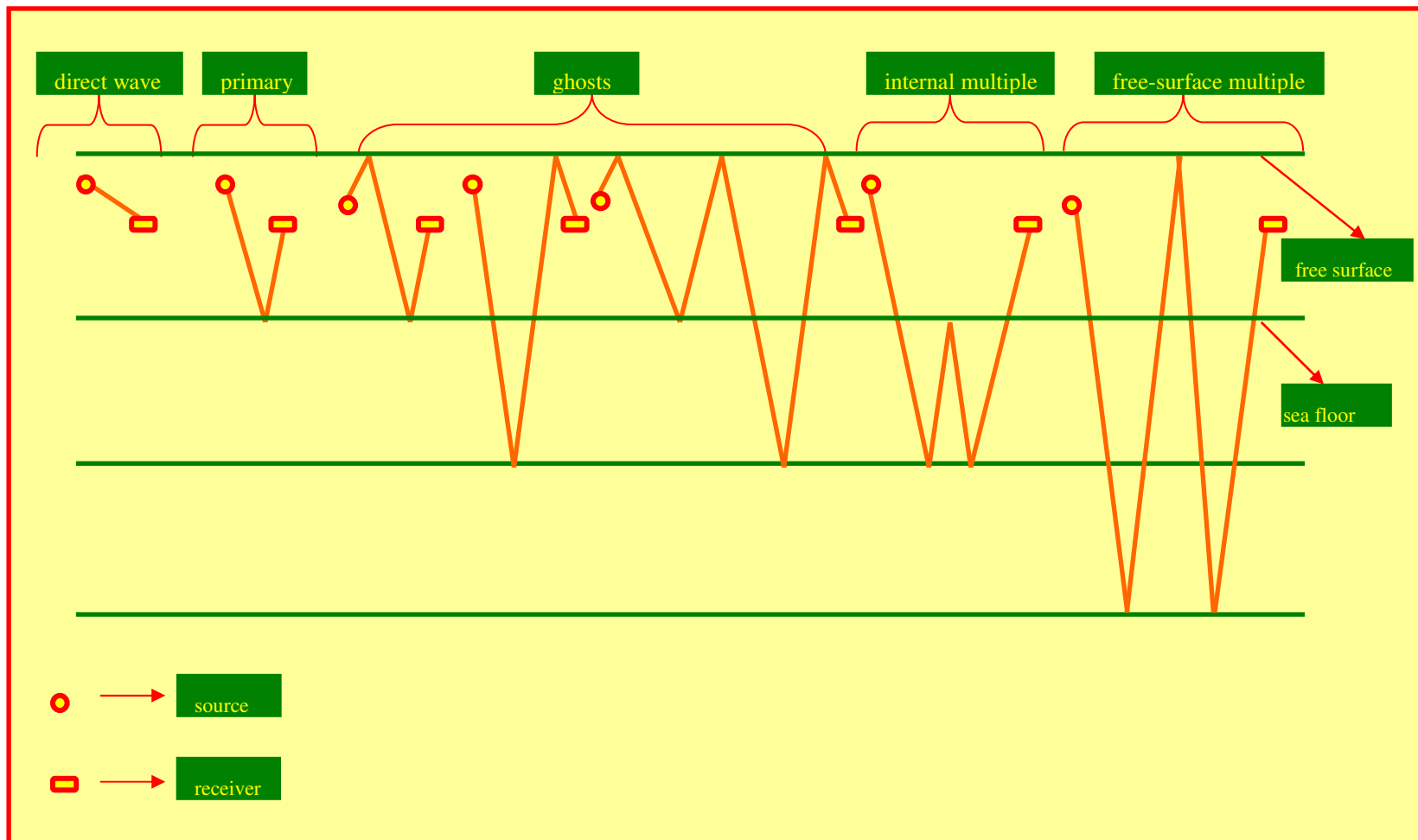


Figure 1.1: An illustration of ray paths common to various seismic events in towed-streamer data.

In thesis we considered a demultiple technique proposed by Ikelle et al. (2004) for free-surface multiple attenuation. The concept of the technique is that a portion of the data containing only primaries must be defined. This is defined by muting the data just above the first free-surface multiples to arrive. The muting location is called the bottom-multiple generator (BMG) reflector (an extensive review is given in Chapter 3).

A multidimensional convolution of the data containing only primaries with the actual data allow for free-surface multiples to be predicted and therefore attenuated.

The big challenge in the application of the BMG demultiple technique is to determine what happen when the mute at the BMG cuts up several seismic events. We investigated the sensitivity by generating synthetic data using the 2D elastic finite difference modeling technique over a complex 2D geology with shallow-water depth, where the deepest water depth of the model is 250 m. Figure 1.2a shows the 2D shallow geology and Figure 1.3a shows the zero offset data of the synthetic data. Note how the free-surface multiples interfere with subsalt layers.

We also investigated, if the weak primaries of the subsalt can be preserved during the demultiple process and if only one step of the BMG demultiple technique would be sufficient to attenuate free-surface multiples. We considered synthetic data generated using the 2D elastic finite difference modeling technique over a complex 2D geology with deep-water depth, where the deepest water depth of the model is 500 m, for the investigation. Figure 1.2b shows the 2D deep geology, and Figure 1.3b shows the zero offset data of the synthetic data. Note the subsalt layers cannot be easily defined due to free-surface multiples interference.

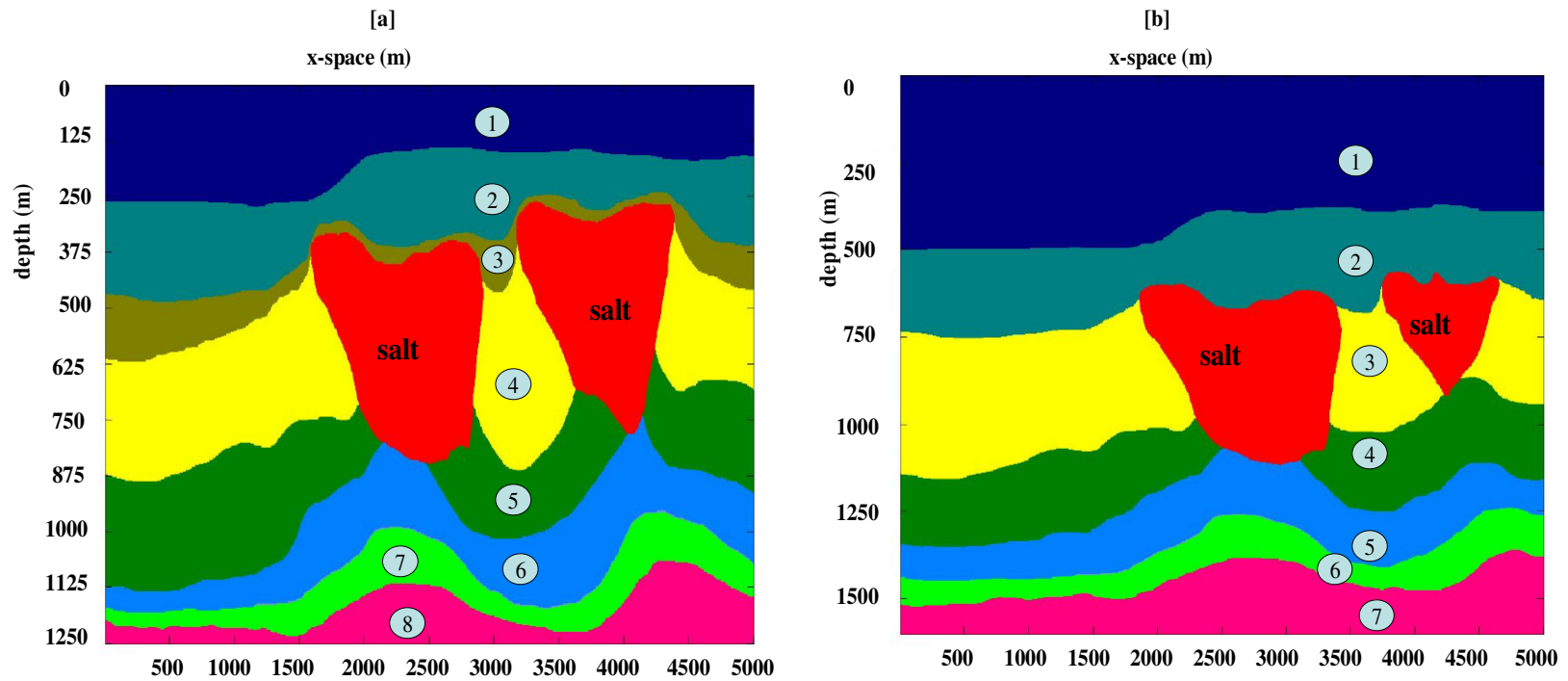


Figure 1.2: The complex 2D geological models (adapted from Lafond et al. 2004) considered for our investigations. The models consist of two isolated salt bodies, which lie close to the seafloor. (a) Shallow-water geology. Layers 5, 6, 7, and 8 are the subsalt layers. (b) Deep-water geology. Layers 4, 5, 6, and 7 are the subsalt layers.

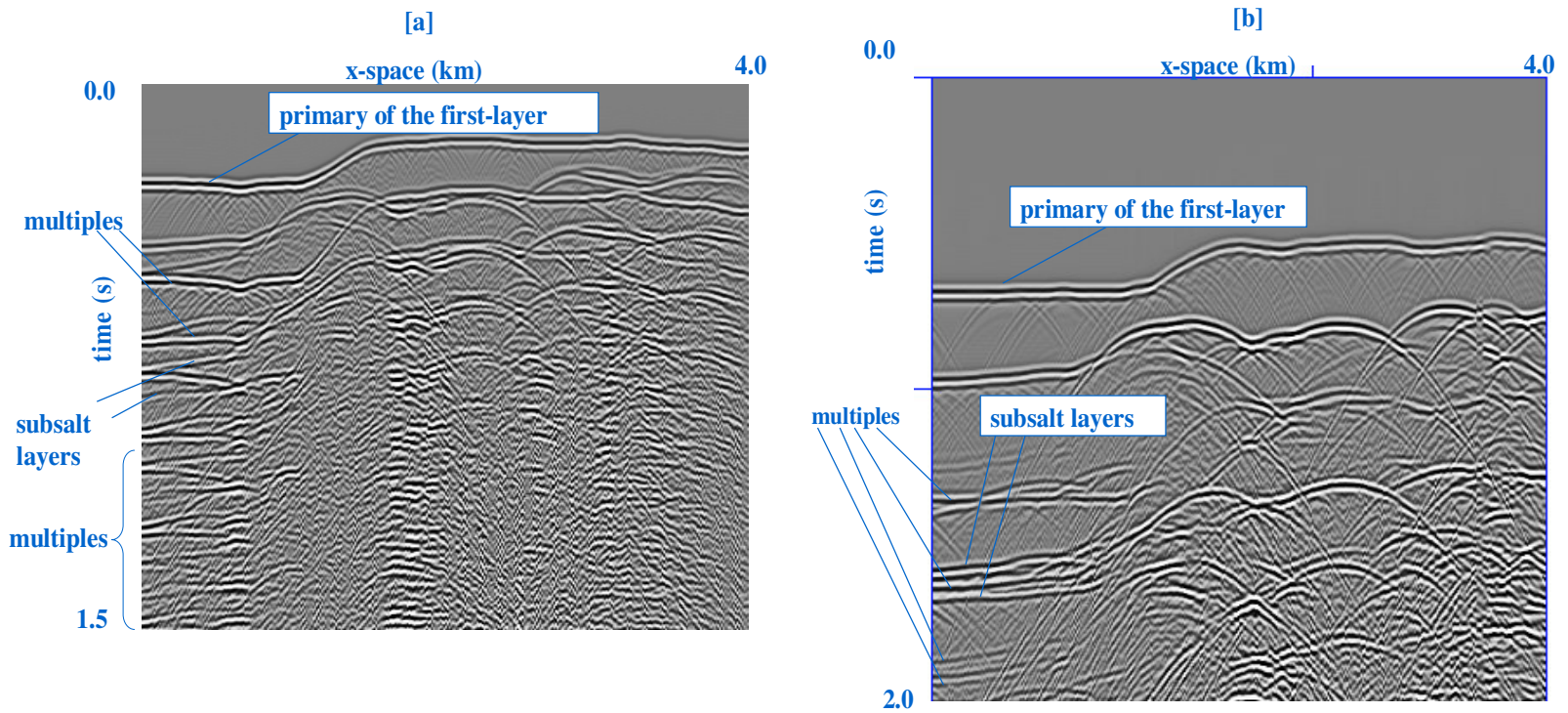


Figure 1.3: Zero offset data before demultiple. (a) Shallow-water geology. (b) Deep-water geology.

## **PROBLEM DESCRIPTION**

### **Multiples**

Multiples are coherent seismic energies that do not follow the ray path of their primaries. Two types of multiples are generated in marine acquisition; these are internal multiples and free-surface multiples.

#### ***Internal Multiples***

Internal multiples are seismic events that have at least one bounce between two layers (Figure 1.4) and no bounce at the free surface interface. Internal multiples usually appear weak in seismic data as compare to the primaries and are hardly visible. As mentioned earlier, the internal multiples are not considered in this thesis.

The orders of the internal multiples depend on the number of bounce between the layers. For example, if there is one bounce between the layers it is called first-order and if there are at least two bounces between layers it is called second-order. Figure 1.4 also illustrates the possible ways that internal multiples can be generated during marine seismic acquisition.

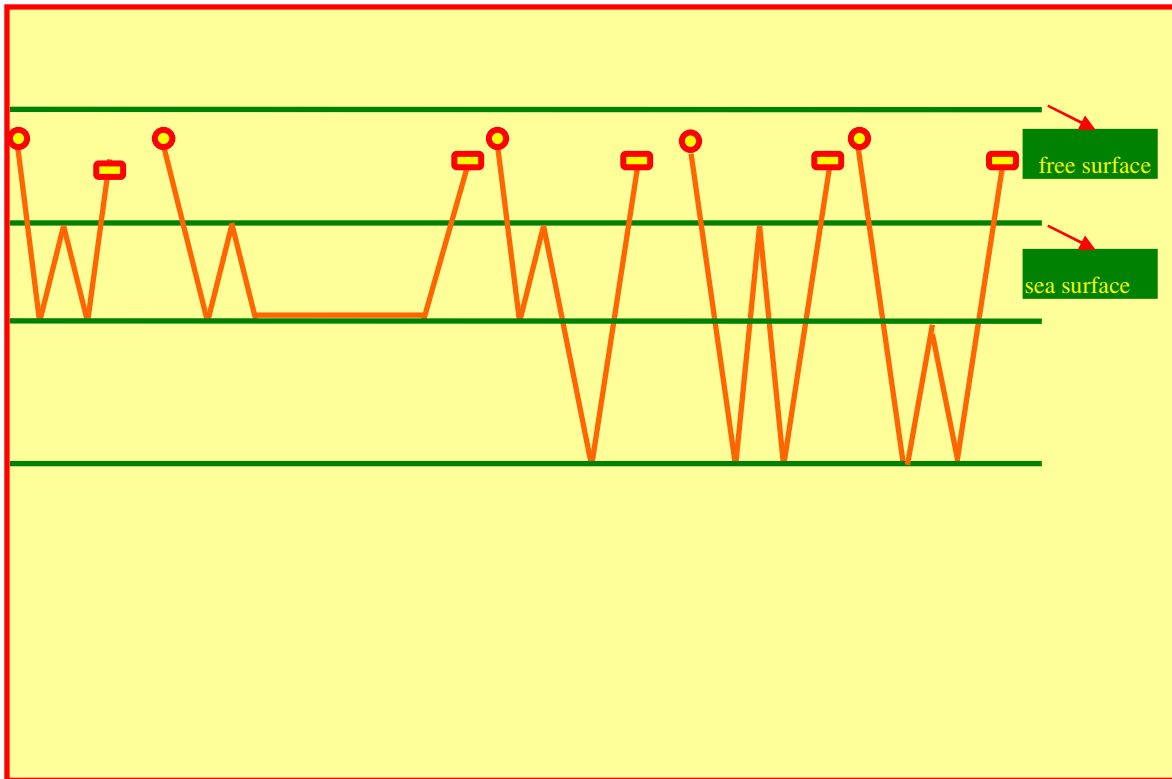


Figure 1.4: An illustration of different types of internal multiples common to marine acquisition.

### ***Free-Surface Multiples***

Free-surface multiples are seismic events that have at least one bounce at the free surface interface. The free-surface multiples like the internal multiples occur in different orders. The orders follow the pattern as described for the internal multiples except that the bounce is at the free surface interface. Figure 1.5 shows an illustration of possible orders of free-surface multiples that can be generated during seismic acquisition although the orders are not limited to the illustration in Figure 1.5.

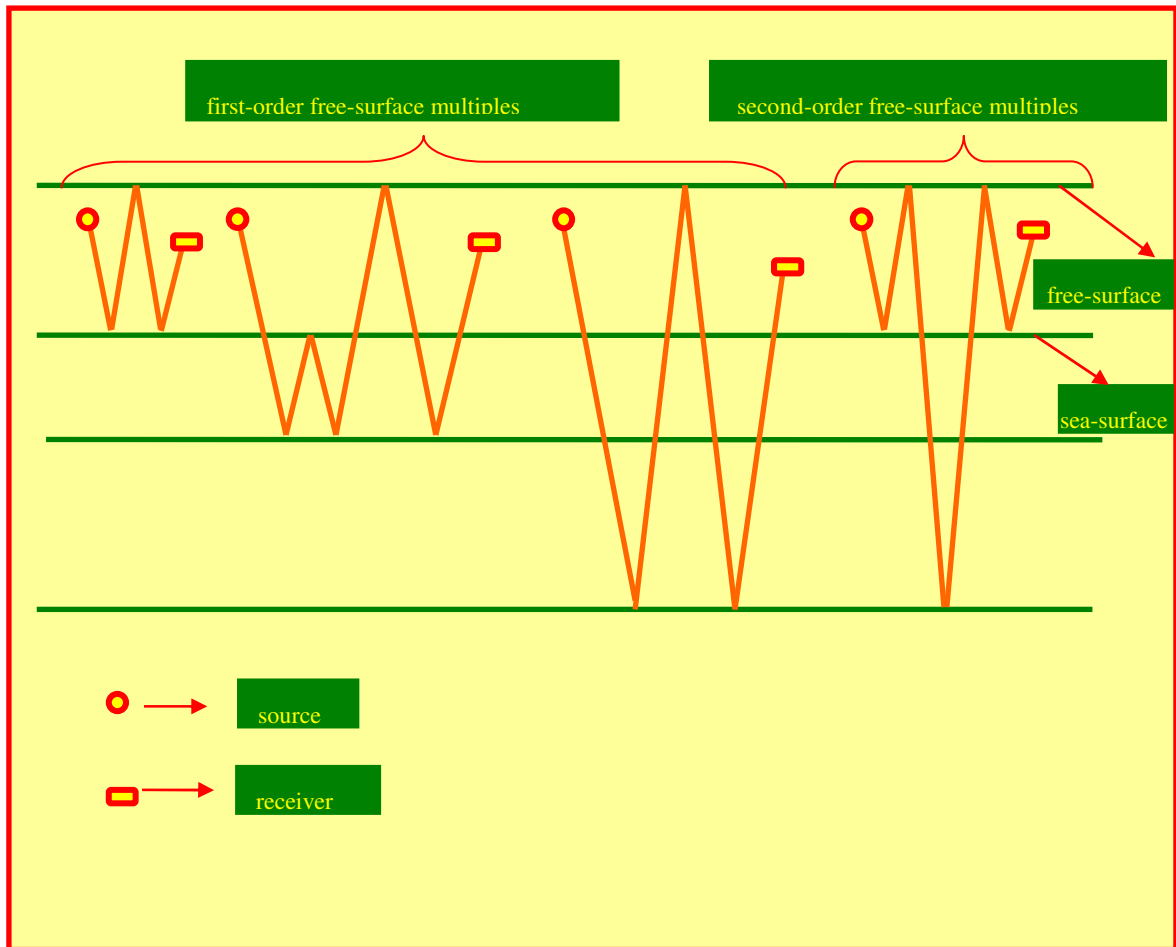


Figure 1.5: An illustration of different types of free-surface multiples common to marine acquisition.

This thesis is focused on attenuating free-surface multiples. Free-surface multiples has pose as a continuous challenge in petroleum seismology. For example, the first-order and second-order free-surface multiples of the primaries of the water-bottom layer can have energies stronger than the primaries of the deeper layers in the subsurface. For this reason, the ability to distinguish the primaries of deeper layers can be very challenging. If the environment is a salt-controlled basin, the weak primaries of the subsalt can hardly be identify because free-surface multiples appears much stronger

and overshadows the weak subsalt primaries.

In complex geology, free-surface multiples interfere with primaries; therefore it is critical to have an attenuation technique that preserves primaries while attenuating free-surface multiples. Also it is very important to attenuate free-surface multiples before imaging in data processing. If the attenuation of free-surface multiples is not carried out, we end up boosting free-surface multiples after imaging. The highly boosted free-surface multiples could be misinterpreted as primaries, which could lead to the drilling of millions of dry holes.

## **A REVIEW OF DEMULTIPLE TECHNIQUES**

Various demultiple techniques have been developed over time. Some of these methods are called the traditional methods. The traditional methods have limitations and because there is more interest in the exploration and production (E&P) industry to explore for oil and gas in complex geology such as subsalt and sub-basalt, new demultiple techniques are being developed to meet with the challenges of multiples attenuation in these types of environments.

Multiple attenuation methods have been classified into different categories by various authors. Weglein (1999), grouped the demultiple techniques into two broad groups. One broad group exploits a feature or properties that differentiate multiples from primaries are under filtering method. The filtering method is sub-divided into two groups, group that exploit periodicity and group that exploits separability of multiples and primaries. Multiple attenuation methods that fall under periodicity are predictive



deconvolution and tau-p ( $\tau - p$ ) transform. Methods that exploit the separability features include common midpoint (CMP) stacking, frequency – wave number (f-k) filter and radon transform.

The second broad group is the wavefield prediction and subtraction technique. Demultiple techniques under the group are the wavefield extrapolation method, the feedback loop and the inverse scattering series.

For this thesis, we categorize the demultiple techniques according to the methods that exploit periodicity, method that exploit separability, and methods that is based on the prediction and subtraction of free-surface multiples.

### **Demultiple Technique Based on Periodicity**

Demultiple techniques that are classified under periodicity are techniques which take advantage of free-surface multiple been periodic. The predictive deconvolution is in this group.

#### ***Predictive Deconvolution***

Predictive deconvolution can be described as a technique that employs the least-square filters with prediction lag greater than unity to predict a seismic event (for example multiples) at a future time. The method depends on three key parameters, the operator length, the prediction lag and the pre-whitening. Some assumptions are considered before the technique can be applied to suppress multiples. It is assumed that the data is zero offset, have minimum phase wavelets, that there are horizontal layers of the subsurface and there are no converted P-S waves. Note that the violation of any of

these assumptions mentioned above, may make free-surface multiples attenuation by the technique questionable.

In practice, there are some criteria, which guide the choice of prediction lag and operator length. The prediction lag should be chosen to bypass the first part of the autocorrelation that represent the wavelets and the operator length should be chosen to include the primaries and the first break of multiples (Yilmaz, 1987).

### **Demultiple Technique Based on Separability**

#### ***CMP Stacking***

The technique takes advantage of the moveout difference between primaries and multiples. Primaries are known to have less moveout than multiples. Normal Moveout (NMO) correction is applied to a common midpoint (CMP) gather using the velocity of the primaries. The primaries flatten out and the free-surface multiples are undercorrected. Hence, the multiples are attenuated during stacking since we use the velocity of the primary to generate the stack.

The CMP stacking fails to attenuate free-surface multiples at near offset data, because the moveout difference between the primaries and free-surface multiples is small.

### ***F-K Filter***

Seismic events in space – time ( $x-t$ ) domain can be separated into different dips in the frequency–wavenumber ( $f-k$ ) domain. The ability to separate events into different dips in the  $f-k$  domain makes it possible to separate and attenuate unwanted signal. To attenuate multiples in the  $f-k$  domain, NMO correction is applied to a CMP gather using a velocity that is in-between the primary velocity and the free-surface multiple velocity. The resulting CMP gather will have the primaries overcorrected and the free-surface multiples undercorrected. This NMO corrected CMP data is transformed into the  $f-k$  domain, where free-surface multiples and primaries are separated into different quadrants. The free-surface multiples lies in the positive quadrant while the primaries lies in the negative quadrant. By zeroing the quadrant where the free-surface multiples lies, data with only primaries is obtained. An inverse Fourier transform is performed to transform the data back to  $x-t$  domain and NMO correction is removed. Figure 1.6 shows an example of  $f-k$  filtering for multiple attenuation.

There is a limitation to the application of the  $f-k$  demultiple. The  $f-k$  demultiple works effectively in attenuating multiples where there exist large dips or moveout between free-surface multiples and primaries but this is not the case in near offset, where there is little moveout between the free-surface multiples and the primaries. Another problem of the  $f-k$  demultiple technique is spatial aliasing. The aliasing of multiples or primaries in the  $f-k$  domain will cause a spill over from one quadrant to another, therefore removing multiples in a single quadrant may leave strong residues of multiples in the data.

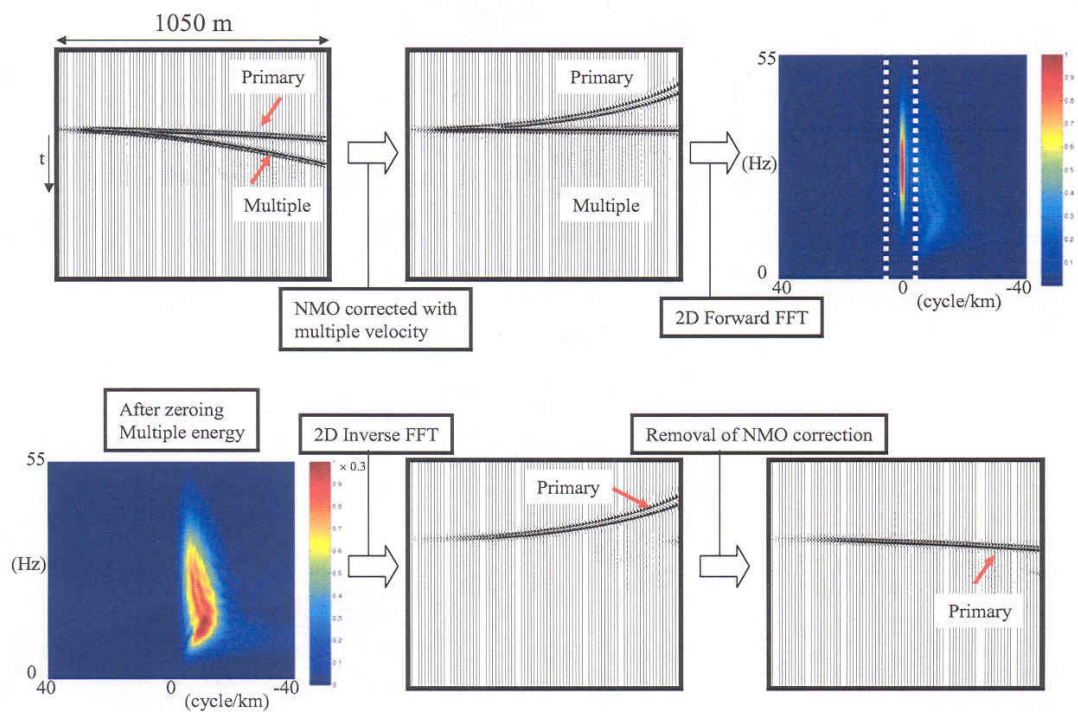


Figure 1.6: An example of f-k filtering for free-surface multiple attenuation (Ikelle and Amundsen, 2003).

### ***Radon Transform***

The radon transform can be defined as the transformation of data from  $(x, t)$  domain to the tau-p  $(\tau, \rho)$  domain. The transformation is carried out via a line integral. Note that the line can be straight, parabolic or hyperbolic.

$$u(p, \tau) = \int dx u(x, \tau + px) \quad (1.1)$$

and

$$t = px + \tau \quad \longrightarrow \quad \text{Linear} \quad (1.2)$$

or

$$t = px^2 + \tau \quad \longrightarrow \quad \text{Parabolic} \quad (1.3)$$

or

$$t = \sqrt{px^2 + \tau^2} \quad \longrightarrow \quad \text{Hyperbolic} \quad (1.4)$$

where  $\tau$  is the intercept time,  $t$  is the time at offset  $x$  and  $p$  is the slowness for hyperbolic and the slowness divided by the distance for parabolic curves.

The limitation of the transform is that it introduces artifacts into the data at near offset.

### **Demultiple Technique Based on Prediction and Subtraction**

#### ***Inverse Scattering Multiple Attenuation (ISMA)***

The inverse scattering multiple attenuation (ISMA) is a multiple attenuation algorithm based on the inverse theory. The series is made up of an infinite sum of terms. Ikelle and Amundsen (1997) represented the series by mathematical notations as:

$$D_p = D_0 + AD_1 + A^2D_2 + A^3D_3 + \dots, \quad (1.1)$$

where  $D_p$  denotes data without free-surface,  $D_0$  is the data with free-surface multiples, the term  $D_1, D_2, D_3, \dots, D_n$  denotes the field of predicted free-surface multiples and  $A$  denotes the source signature. One advantage of the method is that it does not require knowledge of the subsurface and also the amplitudes of primaries are preserved during attenuation process including cases where primaries and free-surface multiples interfere.

One of the limitation of the demultiple method is that it is computational expensive. This is due to the non-linearity in the series, in which the terms  $D_2, D_3$ , etc., are computed several time.

## **SUMMARY**

In summary, a demultiple technique that preserve the primaries, effective at all offset and in complex data and most importantly cost effective is crucial in data processing. In this thesis, we implemented a demultiple technique that is based on the ‘predict then subtract’ approach and the technique satisfies the criteria as mentioned above, that are essential of an effective demultiple technique. The demultiple technique is called the bottom-multiple generator (BMG) reflector approximations.

**CHAPTER II**  
**A BRIEF BACKGROUND ON CONSTRUCTING FREE-SURFACE**  
**MULTIPLES**

**PREDICTION OF FREE-SURFACE MULTIPLES**

Let us review the theory of constructing (predicting) free-surface multiples. According to Ikelle and Amundsen (2003) free-surface multiples can be predicted based on the theory that seismic events can be reconstructed at the scattering point. The scattering point for the reconstruction can be located either at the free surface or in the subsurface, Figure 2.1 shows the possible ways that seismic events can be decomposed.

Note from Figure 2.1 that only free-surface multiples and ghosts can be constructed at the free surface and also from recorded data. This is possible because the free-surface multiples and ghosts split into other seismic events that are already present in the recorded data. The same cannot be said of primaries and internal multiples because both events can be constructed only with the scattering point in the subsurface and then split into events, which have to be extrapolated from the recorded data.

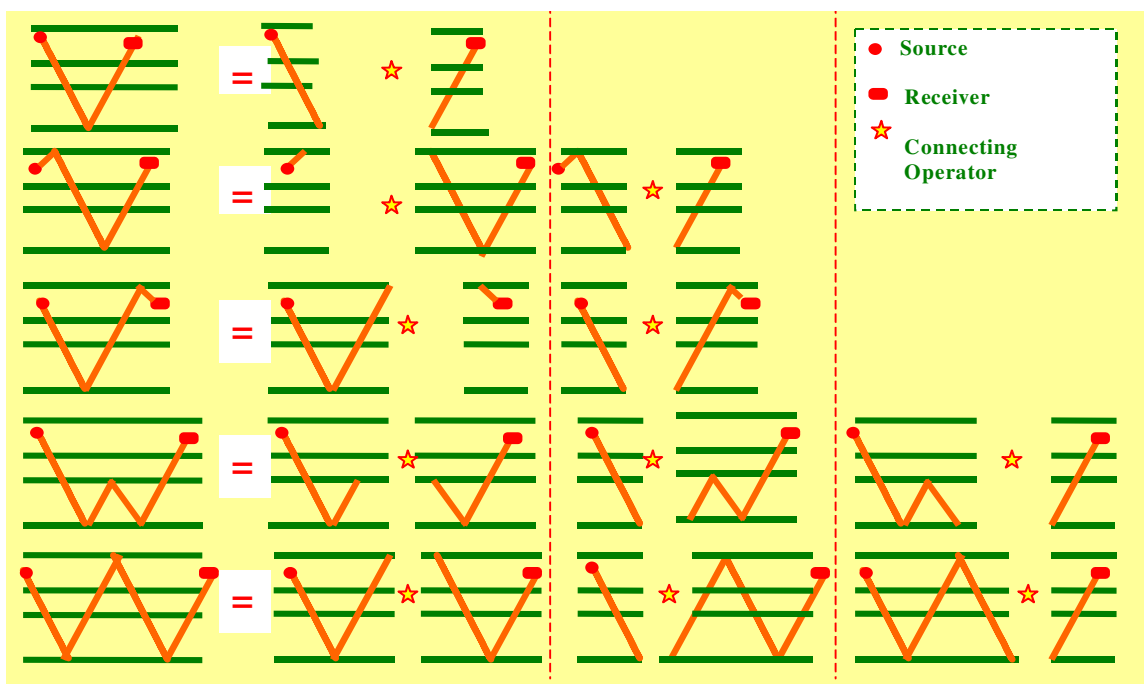


Figure 2.1: An illustration of possible ways in which seismic events can be constructed for towed-streamer data.

We draw the following conclusions based on the theory that has been established, that free-surface multiples can be constructed with the scattering point at the free surface.

- 1) We cannot construct primaries with a scattering point at the free surface.
- 2) We can avoid the construction of ghosts of any seismic events by muting away the direct wave from the data.
- 3) The first-order free-surface multiples can be constructed from a combination of two primaries with one scattering point.
- 4) The second-order free-surface multiples can be constructed from a combination of a primary and the first-order free-surface multiples with one scattering point and can also be constructed from the combinations of three primaries with two



scattering points at the free surface. Note from Figure 2.2 that there are two ways of constructing second-order free-surface multiples with one scattering point and one possible way with two scattering points.

- 5) The third-order free-surface multiples can be constructed from the combination of two first-order free-surface multiples or as a combination of primary and second-order free-surface multiples. Note from Figure 2.2 that there are three possible ways of constructing third-order free-surface multiples with one scattering points, three ways of constructing third-order free-surface multiples with two scattering points and one possible way with three scattering points.

It is essential to recognize that the data have to be extrapolated from the source to the free surface or from the receiver to the free surface before use for the construction of free-surface multiples. This is necessary because acquisition geometry implemented in towed-streamer experiment has the source and the receivers located very close to the free surface (see Figure 2.2).

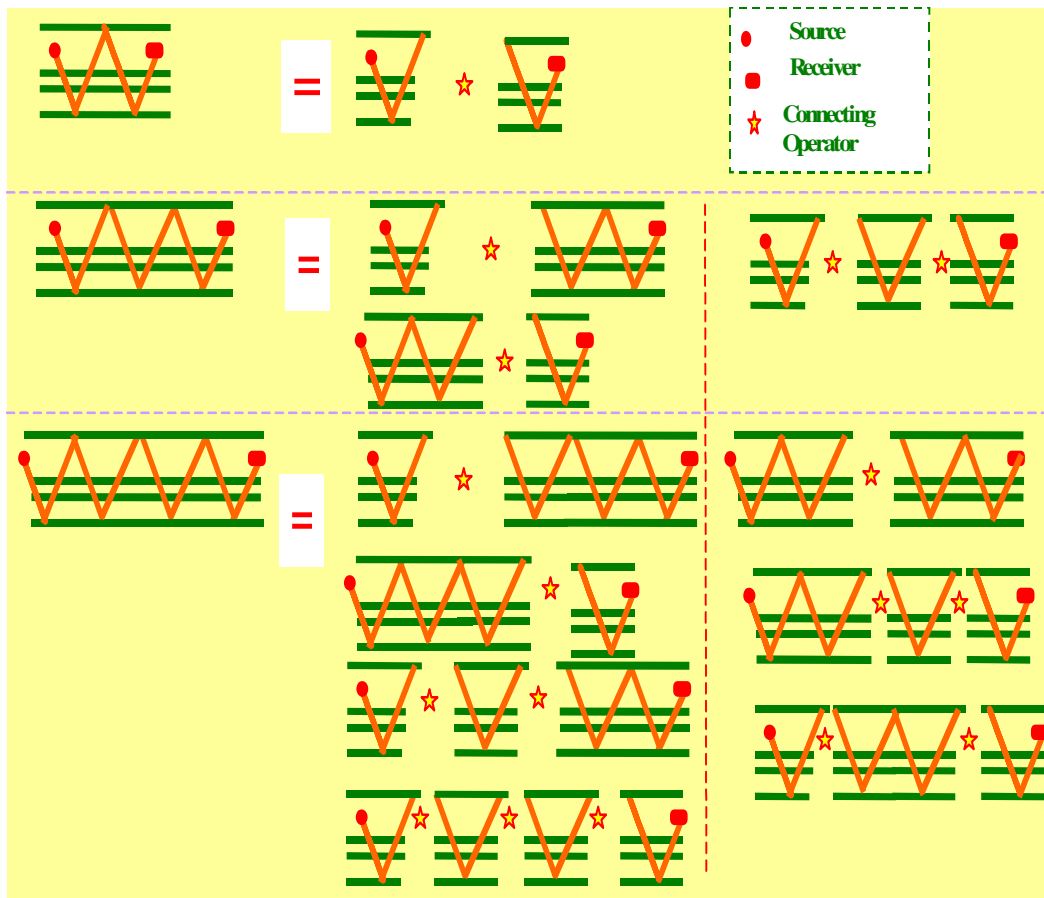


Figure 2.2: An illustration of possible ways in which free-surface multiples can be constructed for towed-streamer data.

**CHAPTER III**  
**CONCEPT OF BOTTOM-MULTIPLE GENERATOR (BMG) REFLECTOR**  
**APPROXIMATION**

**SUBTRACTION OF PREDICTED FREE-SURFACE MULTIPLES**

The predicted free-surface multiples are attenuated from the actual data. Before predicted free-surface multiples can be used for this purpose, it has to be scaled by a scaling factor. The ideal scaling factor is the inverse source signature (a). By scaling the predicted free-surface multiples with the inverse source signature, free-surface multiples can be effectively attenuated because the amplitude and the phase of both the predicted free-surface multiples with free-surface multiples in the actual data is properly adjusted to be equivalent. Unfortunately, the source signature is usually unknown.

Ikelle and Amundsen (2003) explore different methods of obtaining the inverse source signature. One of the methods is to measure the source signature directly. The measurement requires special data acquisition geometries such as the vertical source, dual streamers and so on. Note that the measured source signature is not generally used in practice for the subtraction of predicted free-surface multiples. The reason is that the measured source signature is different from the source signature required to attenuate predicted free-surface multiples. The measured source signature is actually aimed at re-deriving the exact air gun source that was used during seismic acquisition.

Another method is to estimate the inverse source signature that will allow us to attenuate predicted free-surface multiples from the data. The criteria considered for the

estimation of the inverse source signature, is based on the observation that the data without free-surface multiples have less energy than the data with free-surface multiples.

The nonlinear solution to the inverse problem in multiple attenuation is given by equation (3.1)

$$\Phi_p = \Phi_0 + a(\omega)\Phi_1 + a^2(\omega)\Phi_2 + a^3(\omega)\Phi_3 + \dots \quad (3.1)$$

In this thesis we implemented the linear solution to the inverse problem for multiple attenuation. The linear solution is obtained by reducing equation (3.1) to its first two terms in the series, equation (3.2).

$$\Phi_p = \Phi_0 + a(\omega)\Phi_1. \quad (3.2)$$

This is possible because the nonlinearity in the inverse problem is only as a result of the higher polynomial that exists between the inverse source signature  $a(\omega)$  and the data without free-surface multiples.

Ikelle et al. (1997) proposed an approach of estimating the inverse source signature by truncating the series in equation (3.1) to its first two terms in the series, equation (3.2). Ikelle et al. (1997) ended-up with an iterative scheme to compensate for the truncation.

Based on the mentioned criteria, Ikelle and Amundsen (2003) derived a solution to estimate the inverse source signature by reducing equation (3.1) to the first two terms in the series without truncation, equation (3.2). The reduction to equation (3.2) is achieved by defining a portion of the data where there is exist maximum correlation between the free-surface multiples in the data field and the predicted free-surface multiples. Once the desired portion of the data is defined, all other fields of predicted

free-surface multiples ( $\Phi_2, \Phi_3, \dots, \Phi_n$ ) are null.

The approach described above is similar to the truncated series in Ikelle et al. (1997) and therefore we can solve the equation (3.2) and arrive at a stable, noniterative and analytic solution. Let

$$\Phi_p(x_s, x_r, \omega) = \Phi_0(x_s, x_r, \omega) + a(\omega, x_s) \Phi_1(x_s, x_r, \omega) \quad (3.3)$$

where  $\Phi_p(x_s, x_r, \omega)$  denotes data without free-surface multiples,  $\Phi_0(x_s, x_r, \omega)$  denotes recorded data with primaries and free-surface multiples,  $\Phi_1(x_s, x_r, \omega)$  denotes the field of predicted free-surface multiples. Using the least square norm, we minimize  $a(\omega, x_s)$  to

$$S(a) = \|\Phi_p\|^2 + \|a\|^2 \quad (3.4)$$

where

$$\|\Phi_p\|^2 = \int dx_r \int dx_s \int d\omega \Phi_p(x_s, x_r, \omega) W_D(x_s, x_r, \omega) \Phi_p^*(x_s, x_r, \omega) \quad (3.5)$$

and

$$\|a\|^2 = \int d\omega \int \omega' a(\omega) W_a^{-1}(\omega, \omega') a^*(\omega') \quad (3.6)$$

The asterisk (\*) denotes a complex conjugate.  $W_D(x_s, x_r, \omega)$  denotes the weighting function which described the errors in the data and  $W_a(\omega, \omega')$  described the priori information on the source. Note that the term  $\|a\|^2$  is introduced for stability of the solution and the constant  $\sigma^2$  is introduced to the definition of  $\|a\|^2$ , in subsequent inversion formula.

The analytical solution of equation (3.4) is given as

$$a(\omega, x_s) = -\frac{\int d\omega' \int dx_r W_a(\omega, \omega') N(x_s, x_r, \omega')}{\sigma^2 + \int d\omega' W_a(\omega, \omega') Q(x_s, x_r, \omega')},$$

(3.7)

where

$$N(x_s, x_r, \omega') = \Phi_0(x_s, x_r, \omega) W_D(x_s, x_r, \omega) \Phi_1^*(x_s, x_r, \omega) \quad (3.8)$$

and

$$Q(x_s, x_r, \omega') = \Phi_1(x_s, x_r, \omega) W_D(x_s, x_r, \omega) \Phi_1^*(x_s, x_r, \omega). \quad (3.9)$$

Note that  $N(x_s, x_r, \omega')$  is the weighted crosscorrelation and  $Q(x_s, x_r, \omega')$  is the weighted autocorrelation. If  $W_D(x_s, x_r, \omega)$  equals unity, then  $N(x_s, x_r, \omega')$  will be the crosscorrelation between the actual free-surface multiples and the predicted free-surface multiples (See Figure 3.1) and  $Q(x_s, x_r, \omega')$  will be the autocorrelation of the predicted free-surface multiples (See Figure 3.2).

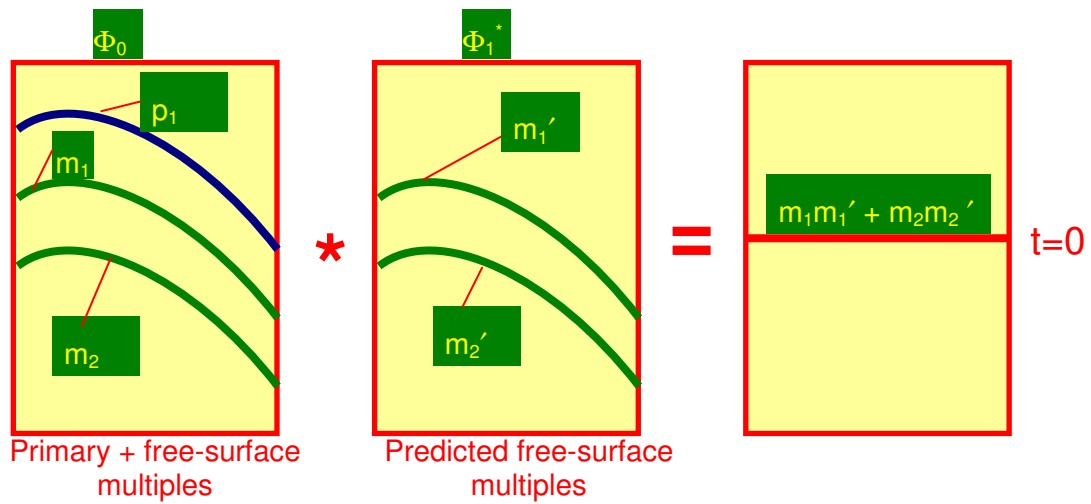


Figure 3.1: An illustration of the crosscorrelation of the actual data containing primaries and free-surface multiples with the predicted free-surface multiples. Note that we are interested in the crosscorrelation of free-surface multiples in the actual data with the predicted free-surface multiples.

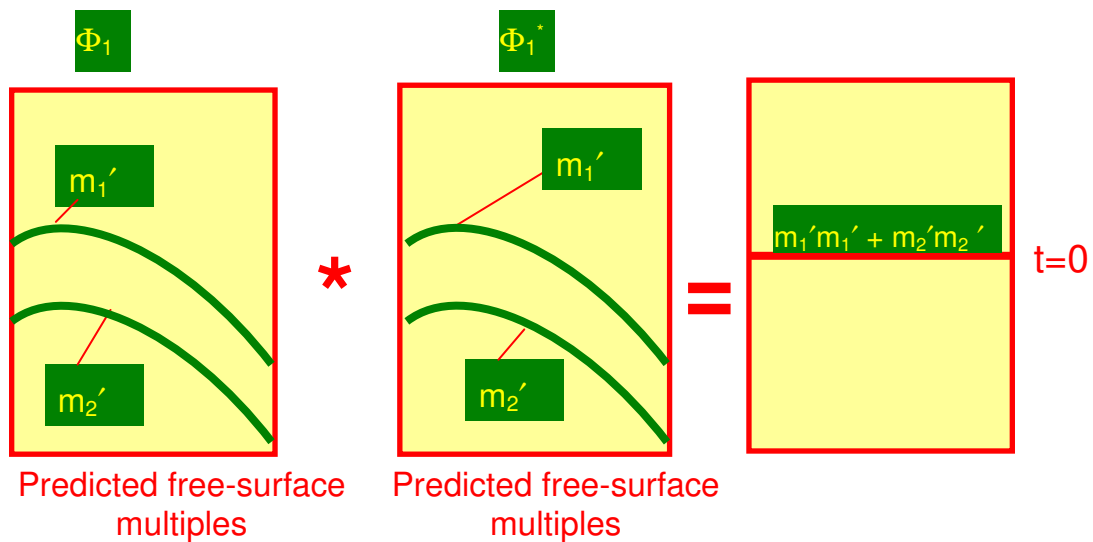


Figure 3.2: An illustration of the autocorrelation of the predicted free-surface multiples.

## REVIEW OF BOTTOM-MULTIPLE GENERATOR (BMG) REFLECTOR APPROXIMATION

Ikelle and Amundsen (2002) proposed a linear solution to the non-linear inverse problem in free-surface multiple attenuation. The Linear solution was obtained by defining a portion of the data that contains only primaries. In the paper, the linear solution was applied to an ocean bottom cable (OBC) data and in another paper was extended to towed-streamer data (Ikelle et al. 2004).

How do we define the data with only primaries? One solution is to define a portion of the data containing only primaries by muting the data just above the first free-surface multiple to arrive. (See Figure 3.3 for the BMG reflector).

The concept of the technique is based on the multidimensional convolution of the portion of the data that contains only primaries with the actual data to predict all orders of free-surface multiples, which will be attenuated from the actual data.

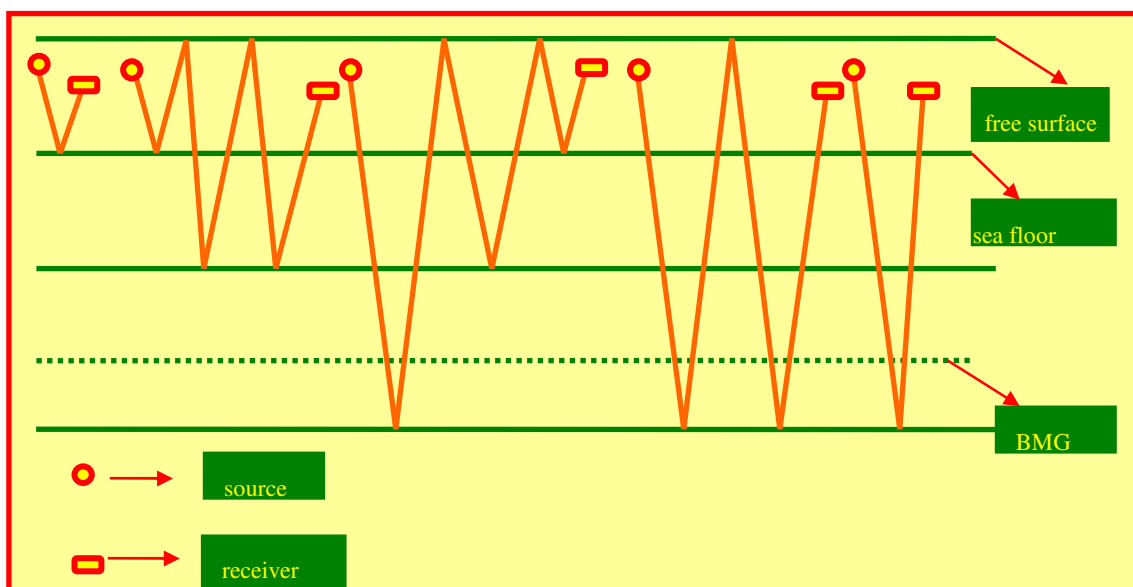


Figure 3.3: The dotted line represents the BMG reflector.



The BMG demultiple technique is can be described as a two-step process. Let us review the two-steps of the demultiple technique as described by Ikelle et al. (2004).

Let the actual data (towed-streamer data) without the direct-wave arrival be denoted by  $\Phi_0 = \{P_0, V_0\}$ , where  $\Phi_0$  denotes the actual data containing primaries and multiples,  $P_0$  denotes the pressure data and  $V_0$  is the vertical particle velocity of the data. Let us also denote the two components of the towed-streamer data containing only primaries as  $\Phi_0^a = \{P_0^a, V_0^a\}$ . Therefore, the first step of the demultiple technique is given by

$$\Phi_{pa} = \Phi_0 + a\Phi_{1a}, \quad (3.10)$$

where the inverse source signature is denoted by  $a$ , and  $\Phi_{1a}$  is the multidimensional convolution of  $V_0^a$  with  $\Phi_0$ . Figure 3.4 shows an illustration of events generated by the multidimensional convolution.

Note from Figure 3.4 that only free-surface multiples that have their first bounce in the subsurface above the BMG reflector are predicted in  $\Phi_{1a}$ .

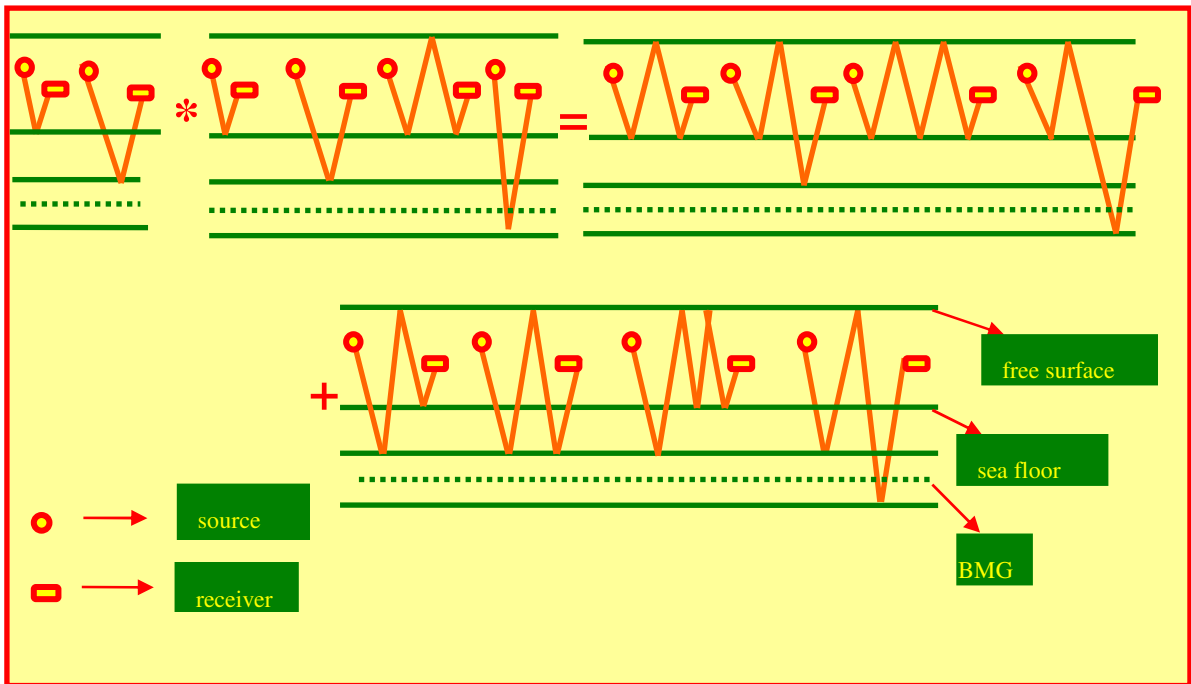


Figure 3.4: An illustration of predicted free-surface multiples obtained from the multidimensional convolution of  $V_0^a$  with  $\Phi_0$ . Note that only free-surface multiples that have their first bounce in the subsurface located above the BMG reflector is predicted and hence attenuated from the actual data,  $\Phi_0$ .

In practice, one way to define the BMG reflector is to take a small portion of the data and perform autoconvolution to produce a data that consist of the first free-surface multiples needed to define the BMG reflector. Figure 3.5 shows an illustration of the events generated from the autoconvolution.

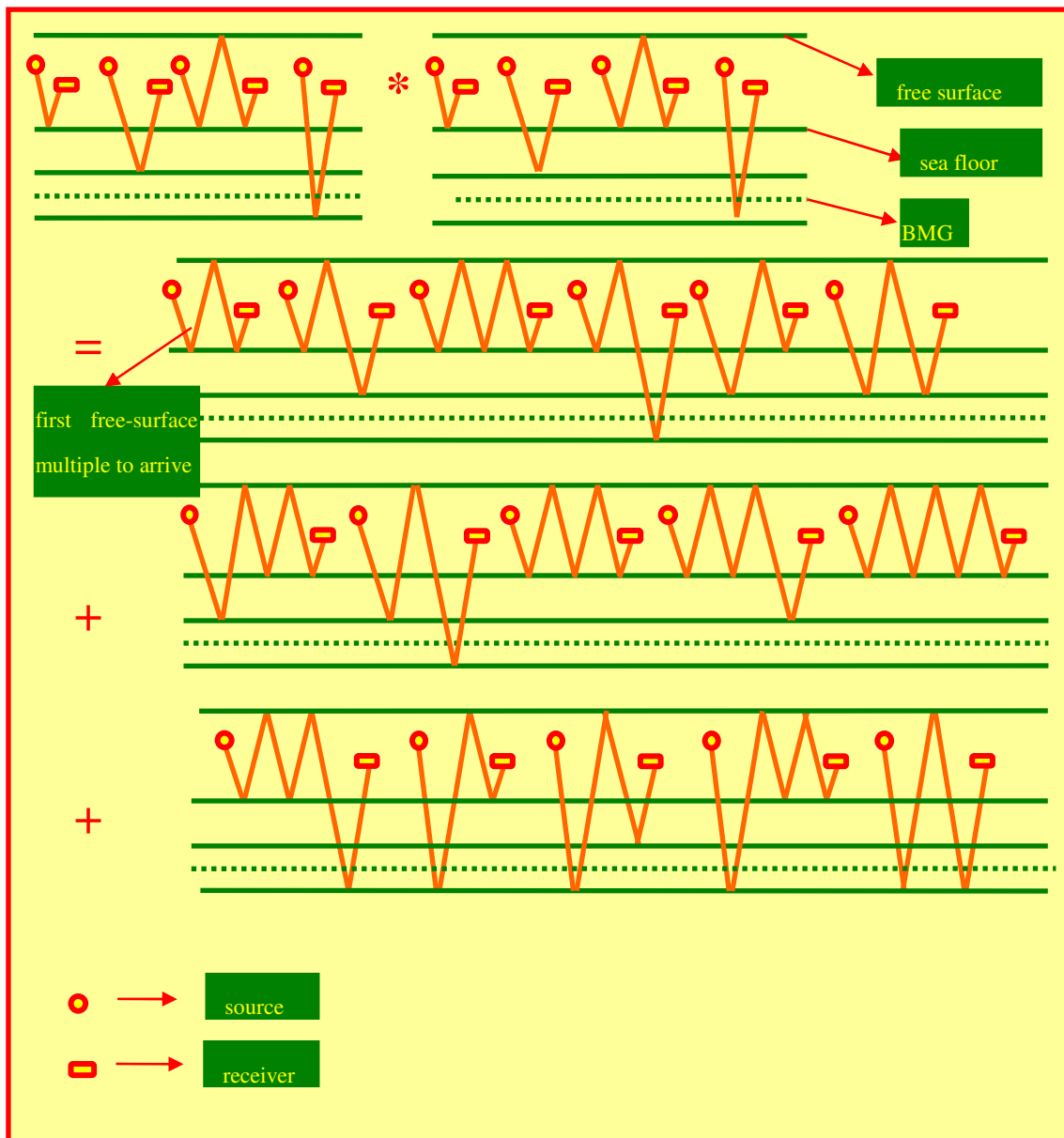


Figure 3.5: An illustration on how the BMG reflector can be define from the autoconvolution of the data.

A second step is required to attenuate free-surface multiples that are still present in  $\Phi_{pa}$ .

Let us denote  $V_{pa}^b$  as a portion of  $V_{pa}$  ( $V_{pa}$  is the vertical particle velocity

corresponding to  $\Phi_{pa}$ ) located below the BMG reflector. The second step of the demultiple technique is given below as

$$\Phi_{pb} = \Phi_{pa} + a\Phi_{1b}, \quad (3.11)$$

where  $\Phi_{1b}$  is the multidimensional convolution of  $V_{pa}^b$  by  $\Phi_0^a$ . Figure 3.6 shows an illustration of events generated by the multidimensional convolution.

Noticed that free-surface multiples with first and last bounces in the subsurface below the BMG reflector are not predicted from the multidimensional convolution (see Figure 3.7 for an illustration of the types of free-surface multiples not predicted in the two steps described above). These types of free-surface multiples are usually weak in deep-water and are hardly visible. There are considered to be as negligible as internal multiples (Ikelle et al. 2004).

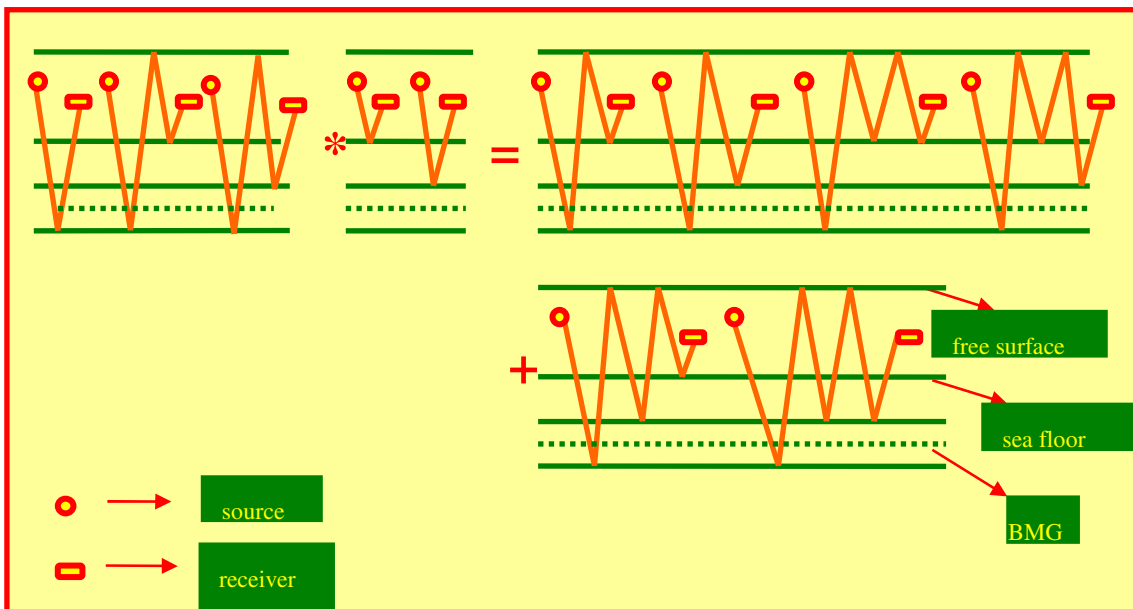


Figure 3.6: An illustration of free-surface multiples predicted from the multidimensional convolution of  $V_{pa}^b$  with  $\Phi_0^a$ .

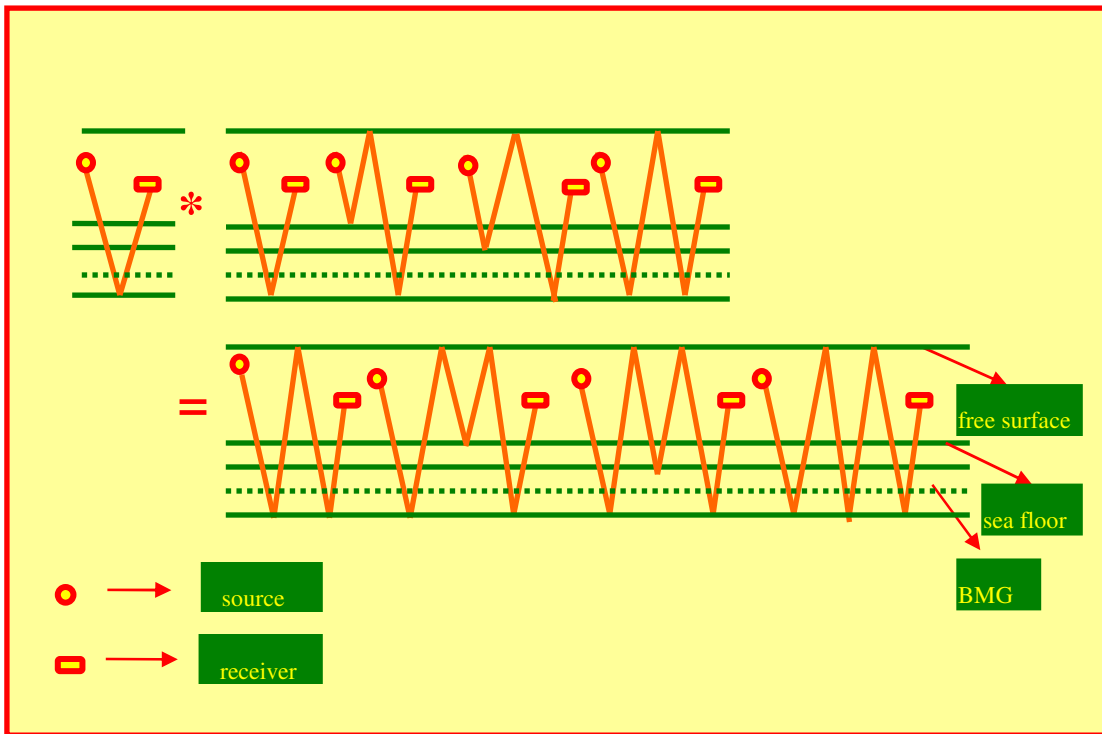


Figure 3.7: An illustration of free-surface multiples not predicted in the two steps of the BMG demultiple technique. Note that these types of free-surface multiples are usually weak in deep-water and are hardly visible.

## HOW TO OBTAIN PARTICLE VELOCITY FROM PRESSURE DATA

In marine acquisition, especially towed-streamer, the parameter recorded is the pressure data. The BMG demultiple technique requires the vertical velocity of the data to perform the multidimensional convolution which predict free-surface multiples.

One way of obtaining the vertical component of the particle velocity is to numerically compute it from the pressure data. Ikelle and Amundsen (2003) describe the computation as follows:

$$V'_z(k_x, k_y, z_s, \omega, x_r) \approx \sigma_0 \frac{k_z}{\omega} P_0(k_x, k_y, z_s, \omega, x_r), \quad (3.12)$$

with

$$k_z = \sqrt{\frac{\omega^2}{c^2} - k_x^2 - k_y^2}, \quad (3.13)$$

where  $k = (k_x, k_y)$  denotes the wavenumbers for the horizontal coordinates  $\chi = (x, y)$  and  $V'_z(k_x, k_y, z_s, \omega, x_r)$  and  $P_0(k_x, k_y, z_s, \omega, x_r)$  are the Fourier transforms of  $V'_z(\chi, z_s, \omega, x_r)$  and  $P_0(\chi, z_s, \omega, x_r)$  with respect to  $\chi = (x, y)$  respectively.

## POTENTIAL ERRORS

The potential errors that can be related to the BMG demultiple technique can be classified into the modeling error and the prediction error.

The modeling errors occur in the course of computing the predicted free-surface multiples. These errors can be measured by analyzing the time delays between the predicted free-surface multiples and the free-surface multiples from the actual data. The time delays is computed from the normalized crosscorrelation of the predicted free-surface multiples with the free-surface multiples for a defined small portion of the actual data, made at  $J$  time samples and  $I$  traces, around  $(x, t)$ , Ikelle and Amundsen (2003). The normalized crosscorrelation can be described as the ratio of the crosscorrelation between the actual data and the predicted free-surface multiples to the autocorrelation of the predicted free-surface multiples.

When the free-surface multiples from the actual data and the predicted free-surface multiples are in phase everywhere, we usually assume accurate modeling of the predicted free-surface multiples. Note that the modeling error map ignores the amplitude

errors that can occur in the predicted free-surface multiples but if the modeling error map is use alongside with the subtraction error map (which would be discussed later in this subsection), potential amplitude error can be identified.

The second errors that can be observed with the BMG demultiple technique is the subtraction errors. We can measure these errors from the evaluation of the correlation energies between the predicted free-surface multiples and the actual data before and after demultiple. With this comparison it is easy to identify where residues of free-surface multiples are present in the data.

As earlier mentioned, when we use both the modeling error map along with the subtraction error map, we can observe amplitude errors in the predicted free-surface multiples. Also by using both maps together, we can have an idea of what type of errors is being experienced. For example, if the time delay in a particular area of the data is not consistent with the common trend of the data, and the correlation energies between the predicted free-surface multiples and the actual data, after demultiple remain the same as before demultiple, then the error can be attributed to modeling of the predicted free-surface multiples.

If the time delay is consistent in very part of data but the correlation energies between the predicted free-surface multiples and the actual data after demultiple remain the same as before demultiple, then the error maybe due to either amplitude error of the predicted free-surface multiples or the subtraction technique that was implemented.

Usually the energy residues observed in the correlation of energies can be due to the interference of free-surface multiples and primaries. If the window over which the

crosscorrelation and the autocorrelation is performed is increased, the energy that may be due to the interference of free-surface multiples and primaries can be discriminated.

## **CONCLUSIONS**

### **Novelty and Importance of the BMG Demultiple Technique**

- 1) No knowledge of the subsurface is required.
- 2) The BMG demultiple technique is effective at all offset and in complex data, therefore it can be used to attenuate free-surface multiples in any environment.
- 3) There are savings in the cost of computation of the series, data storage, and computation time as compared to the nonlinear solution of the inverse problem.



**CHAPTER IV**  
**ANALYSIS OF EFFECT OF BOTTOM-MULTIPLE GENERATOR (BMG)**  
**APPROXIMATION IN COMPLEX GEOLOGY**

**GEOLOGICAL MODELS DESCRIPTION**

The complex 2D geological models considered for the demonstration of the effectiveness and sensitivity of the BMG demultiple technique both contained isolated salt bodies, which lie close to the seafloor. Note that the seafloor is irregular. The difference between the complex 2D geological models is that one model has shallow-water depth (deepest depth is 250 m) while the other model has deep-water depth (deepest depth is 500 m). Figures 4.1 and 4.2 shows the complex 2D geological models respectively.

We designed the shallow-water depth geological model so that we can demonstrate that the BMG demultiple technique will be effective in attenuating free-surface multiples even when the mute at the BMG location cut-up several seismic events for example the primaries. With the shallow-water depth geology, we can generate primaries that are needed to predict free-surface multiples to have their trajectories crossing the BMG location. This may be the same scenario in complex geology.

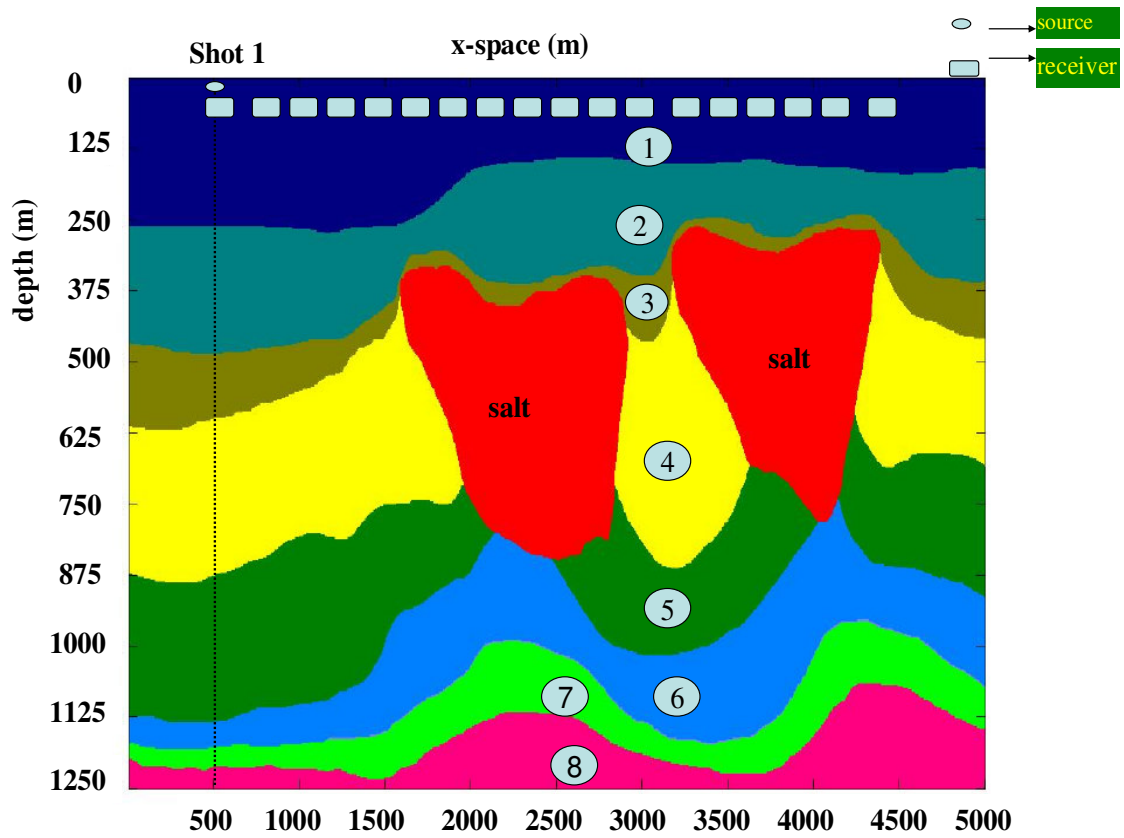


Figure 4.1: Complex 2D shallow-water depth geology (adapted from Lafond et al. 2004) considered for our investigation of the BMG demultiple technique (Case I). Layers 5, 6, 7, and 8 are the subsalt layers.

Table 4.1: Modeling parameters of the subsurface layers in Figure 4.1

Layer	$V_p$ (m/s)	$V_s$ (m/s)	$\rho$ (g/cc)
1	1500	0	1.00
2	1950	969	2.00
3	2257	1200	2.30
4	2450	1400	2.50
5	2300	1200	2.20
6	2607	1350	2.30
7	3000	1600	2.45
8	2800	1450	2.67
Salt	4400	1800	2.20

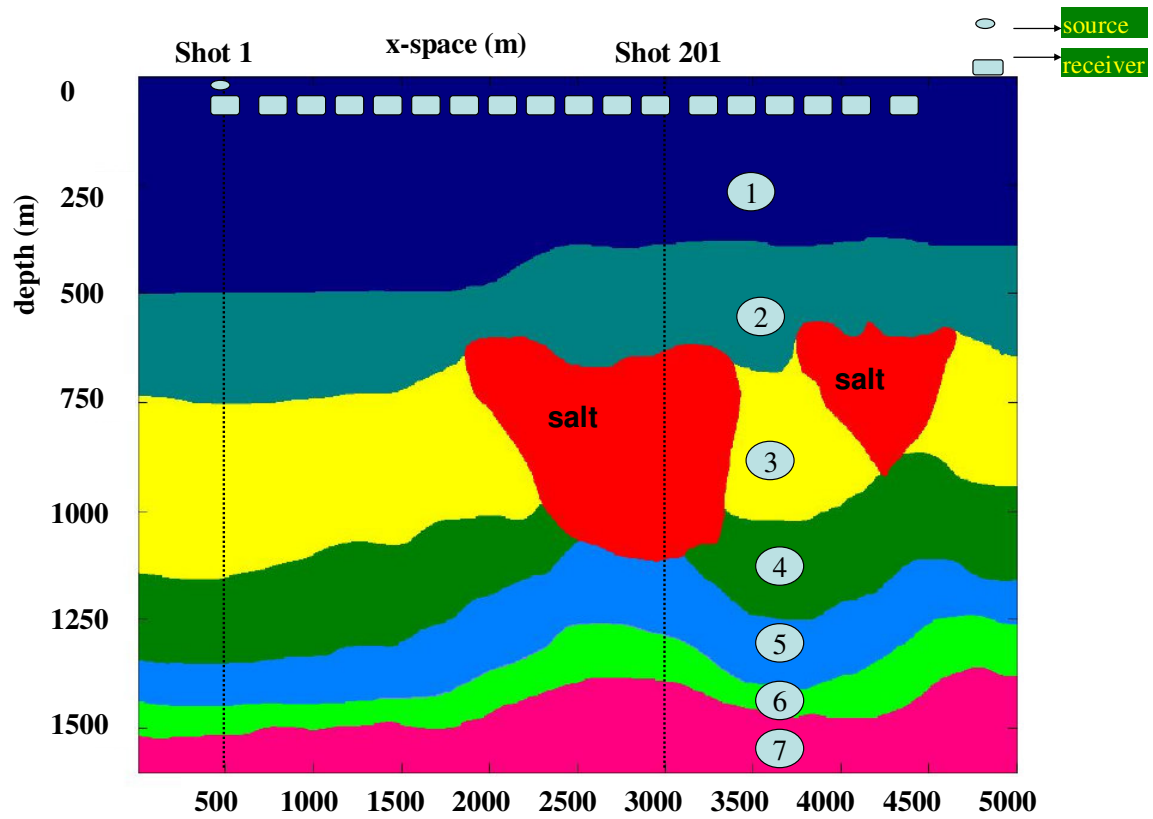


Figure 4.2: Complex 2D deep-water geology (adapted from Lafond et al. 2004) considered for our investigation of the BMG demultiple technique (Case II). Layers 4, 5, 6 and 7 are the subsalt layers.

Table 4.2: Modeling parameters of the subsurface layers in Figure 4.2

Layer	$V_p$ (m/s)	$V_s$ (m/s)	$\rho$ (g/cc)
1	1500	0	1.00
2	1800	669	1.50
3	1900	795	2.00
4	2000	1150	2.20
5	2607	1350	2.30
6	3000	1600	2.45
7	2800	1450	2.67
Salt	4400	1800	2.20

The deep-water geology was designed to demonstrate the effectiveness of the BMG demultiple in deep-water and to show that the first step of the BMG demultiple technique can adequately attenuate most of the free-surface multiples. According to Ikelle et al. (2004), when the BMG location is deep enough, only one step of the demultiple technique may be required. Hence, the data above the BMG location should not be shallow, and if shallow, the BMG location can be lowered.

## **APPLICATION OF BMG DEMULTIPLE TECHNIQUE**

### **Case I: Shallow-Water Geology**

We generated 321 shots using the 2D elastic finite difference modeling technique. Each shot had a shot interval of 12.5 m, shot over a distance of 4 km, and the depth of the source in water is 5 m. Table 4.1 shows a detail of the modeling parameters used for data acquisition.

We applied the two steps of the BMG demultiple technique to the synthetic data generated. We considered the shot located at 500 m (see Figure 4.1 for the shot location) for our analysis. We chose this shot because it is a good representation of salt reflections and reflections at all offsets. (Figure 4.3 is the shot gather of the shot located at 500 m, which is an example of the actual data  $\Phi_0$  ).

The first step of the BMG technique has explained in the previous Chapter, is to define the portion of the data containing only primaries by muting the actual data just above the first free-surface multiples. Figure 4.4 is an example of data containing only primaries,  $V_0^a$ . Note that the primaries of the top salt as well as the primaries of the first

and second layers are cut up at the BMG location.

The multidimensional convolution of  $V_0^a$  with the actual data  $\Phi_0^a$  predicts  $\Phi_{1a}$ .  $\Phi_{1a}$  contains free-surface multiples whose first bounce in the subsurface are located above the BMG reflector. Figure 4.5 is an example of  $\Phi_{1a}$ . Note that the primary of the top of the salt cut up at the BMG location has been partially predicted.  $\Phi_{1a}$  is attenuated from the data when equation (3.10) is applied to obtain a demultiple result,  $\Phi_{pa}$ , Figure 4.6. Note that free-surface multiples interfering with the primaries at about 1.77s have been attenuated, and the primaries have been preserved. Also note that only the free-surface multiples predicted in  $\Phi_{1a}$  are attenuated from the actual data  $\Phi_0$ . Therefore, the second step of the BMG demultiple technique described in the previous chapter by equation (3.11) is applied to attenuate the free-surface multiples still present in  $\Phi_{pa}$ .

We defined the portion of the particle velocity below the BMG reflector  $V_{pa}^b$  (Figure 4.7), where  $V_{pa}^b$  is the particle velocity components of  $\Phi_{pa}$ . The multidimensional convolution of  $V_{pa}^b$  with the portion of the actual data located above the BMG reflector predicts free-surface multiples whose first bounce in the subsurface is located below the BMG reflector,  $\Phi_{1b}$ . Figure 4.8 is an example of  $\Phi_{1b}$ . Note that the other portion of the primary of the top of the salt is predicted.

After we applied equation (3.11), we obtained a final demultiple result  $\Phi_{pb}$  (Figure 4.10).

We compared Figure 4.9, where Figure 4.9 is the shot gather of shot located at 500 m before demultiple (same as Figure 4.3) to Figure 4.10. Note that in Figure 4.10 free-surface multiples have been effectively attenuated. The free-surface multiples residues in the data are free-surface multiples not predicted by the two steps of the BMG demultiple technique. Figure 3.7 is an example of these types of free-surface multiples.

The type of free-surface multiples described in Figure 3.7 are hardly visible in a deep-water environment, but because the water depth of the geological model used for our demonstration of the BMG demultiple technique is shallow in this case, the free-surface multiples residues are visible. Note that the BMG should not be shallow, and if it is, the BMG location should be lowered to the second order free-surface multiples to arrive.

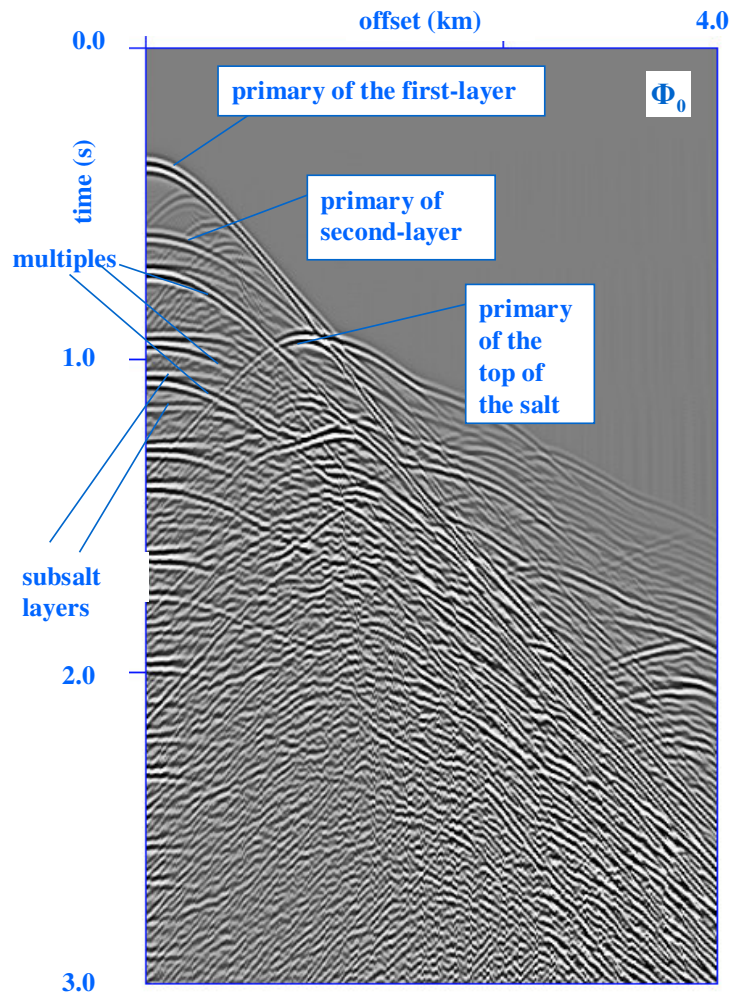


Figure 4.3: Shot gather of shot located at 500 m considered for our analysis.

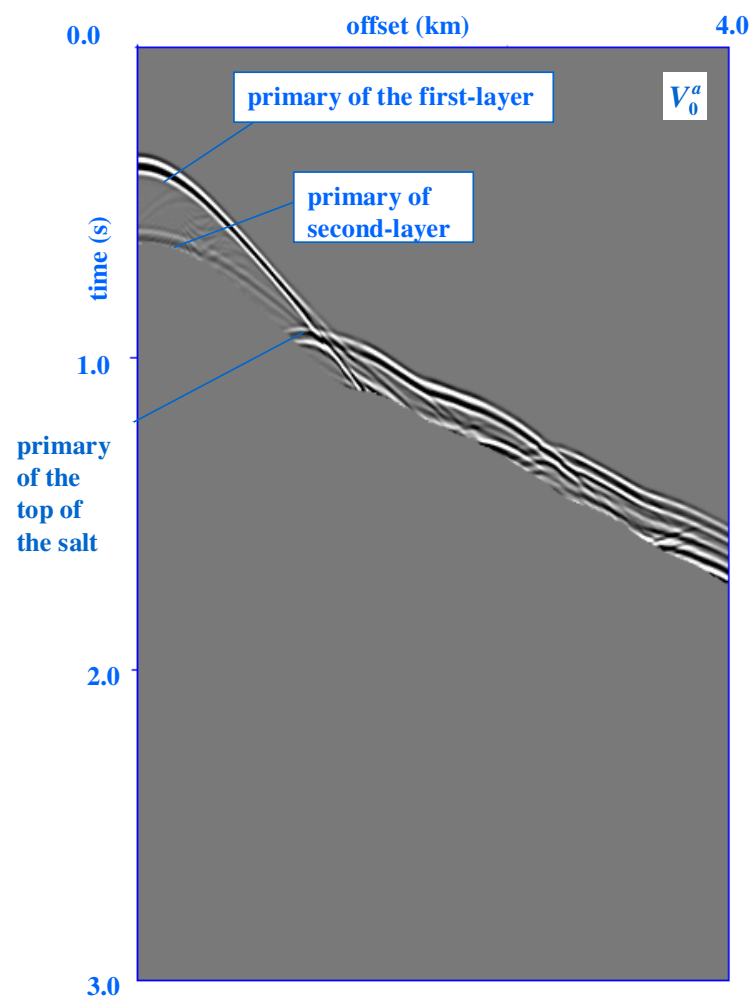


Figure 4.4: An example of data containing only primaries located above the BMG reflector.

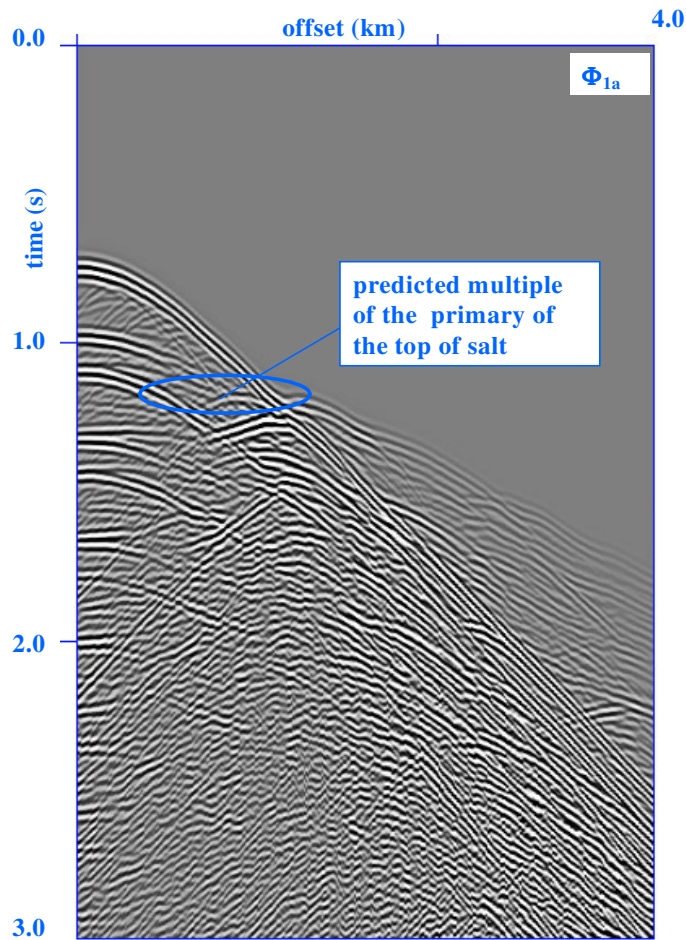


Figure 4.5: An example of the field of predicted free-surface multiples obtained from the multidimensional convolution of  $V_0^a$  with  $\Phi_0$ .

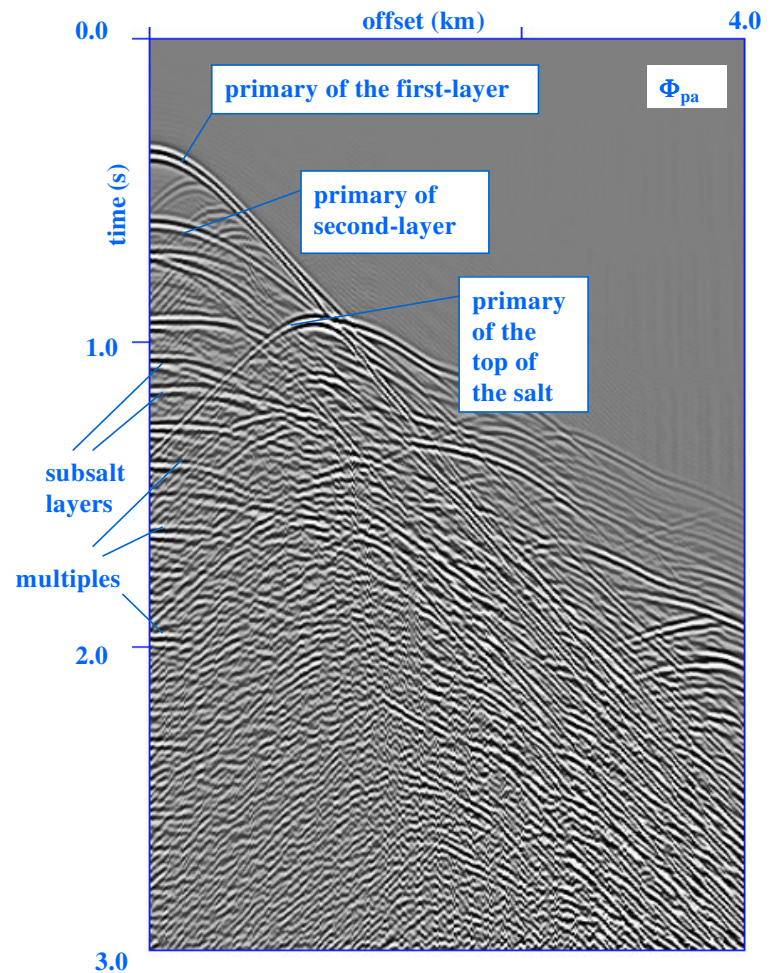


Figure 4.6: The first demultiple result obtained after the application of the first step of the demultiple technique.



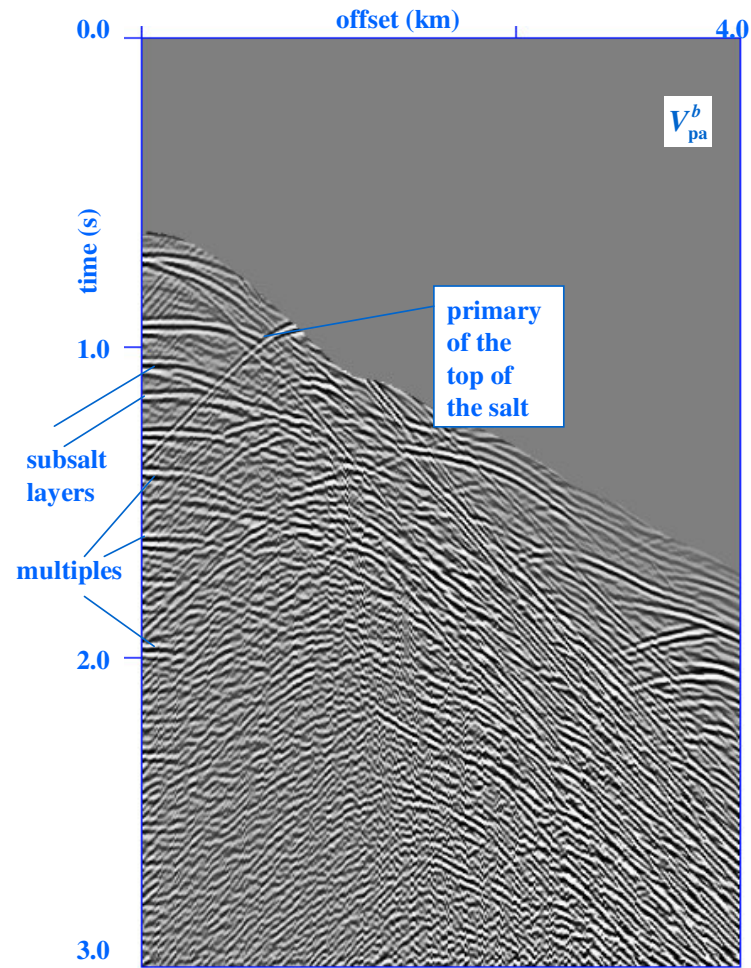


Figure 4.7: An example of the data located below the BMG reflector.

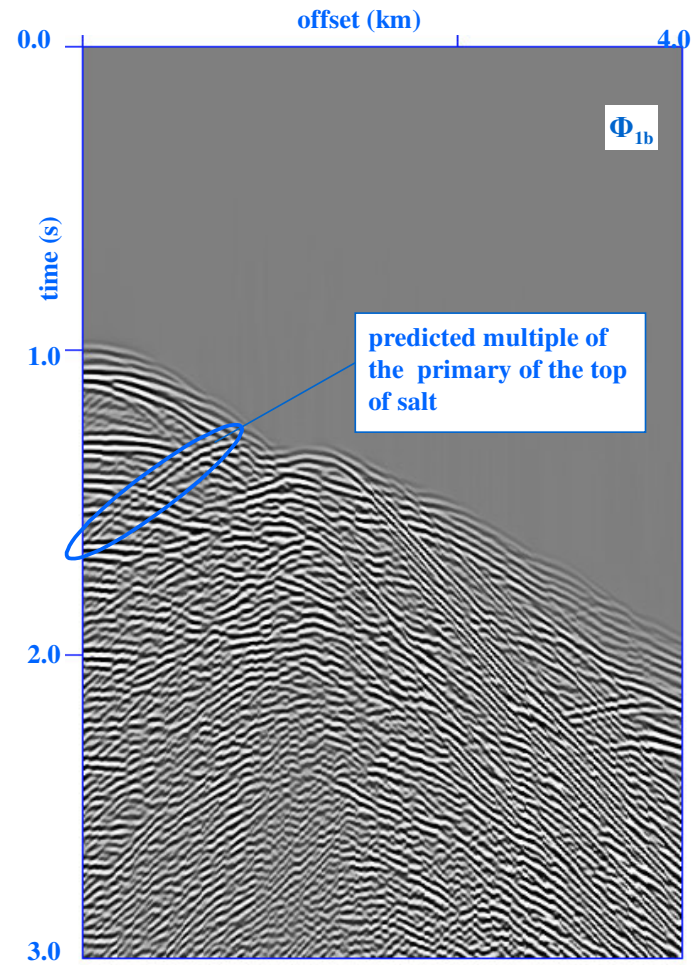


Figure 4.8: An example of the field of predicted free-surface multiples obtained from the multidimensional convolution of  $V_{pa}^b$  with  $\Phi_0^a$ .

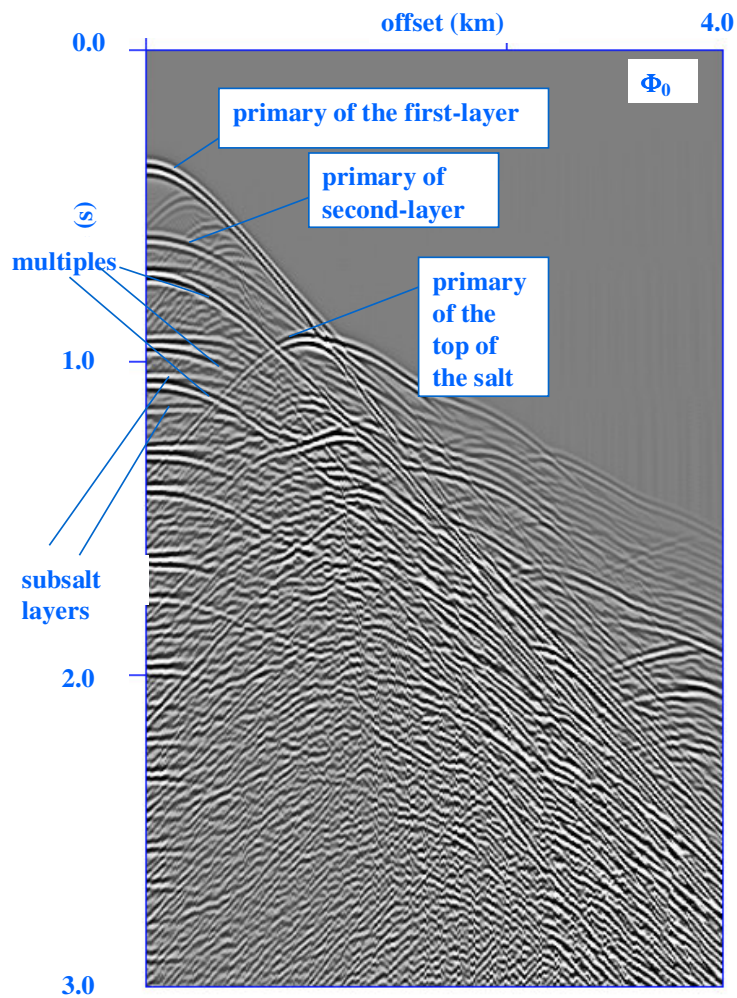


Figure 4.9: An example of the actual data from shot located at 500 m.

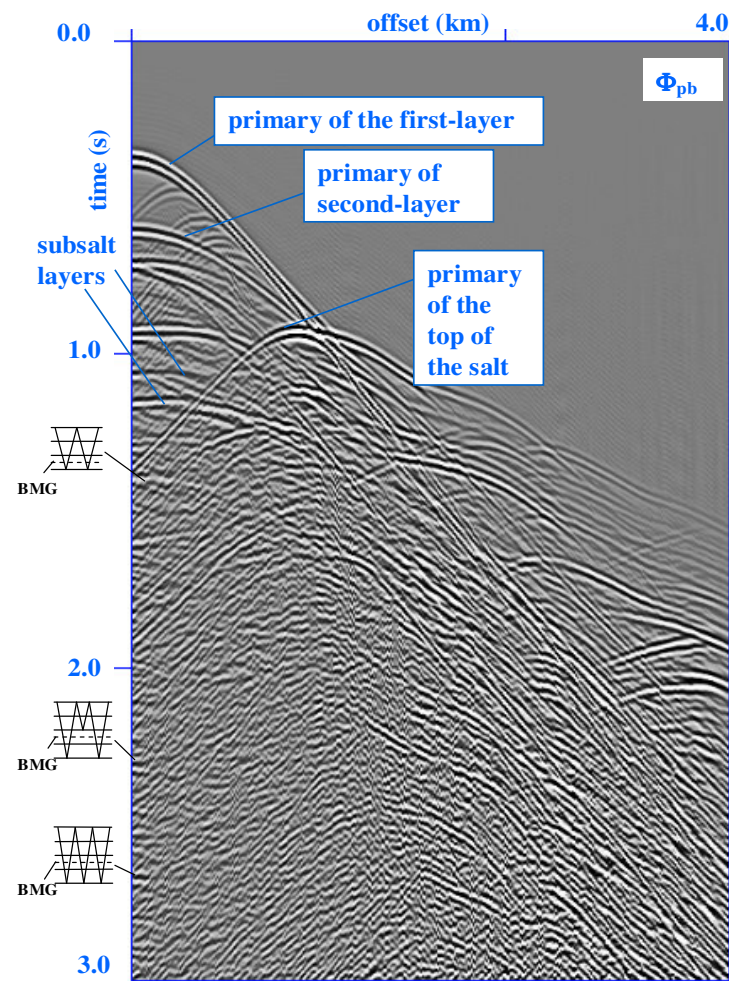


Figure 4.10: An example of the final demultiple result after the application of the second step of the BMG demultiple technique.

We have also compared zero offset data before and after the demultiple to further aid our analysis. Figure 4.11 shows the zero offset data before the demultiple. Note the interference of free-surface multiples with primary of the subsalt. Figure 4.12 shows the zero offset data after applying the first step of the demultiple technique. Note the presence of free-surface multiples, which are not attenuated in the first step of the demultiple technique. Some of these multiples have arrival time, which is early in the section. Figure 4.13 shows the final demultiple result after the application of the second step of the demultiple technique. Noticed that free-surface multiples have been effectively attenuated, and the mute at the BMG location does not affect the primary reflections of top of salt, the first, and second layers, which cut through these events. Also notice that the weak subsalt reflections can be defined compare to before the demultiple.

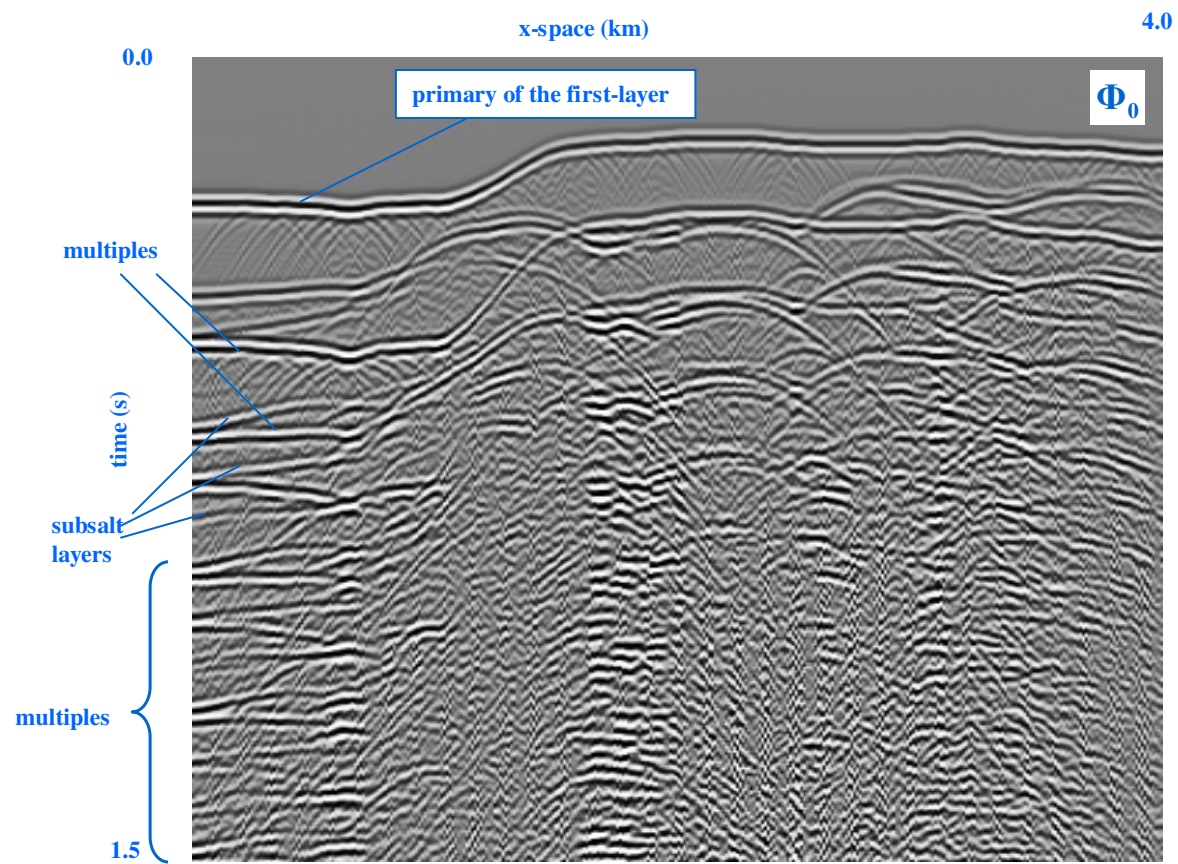


Figure 4.11: Zero offset data of the actual data before demultiple.

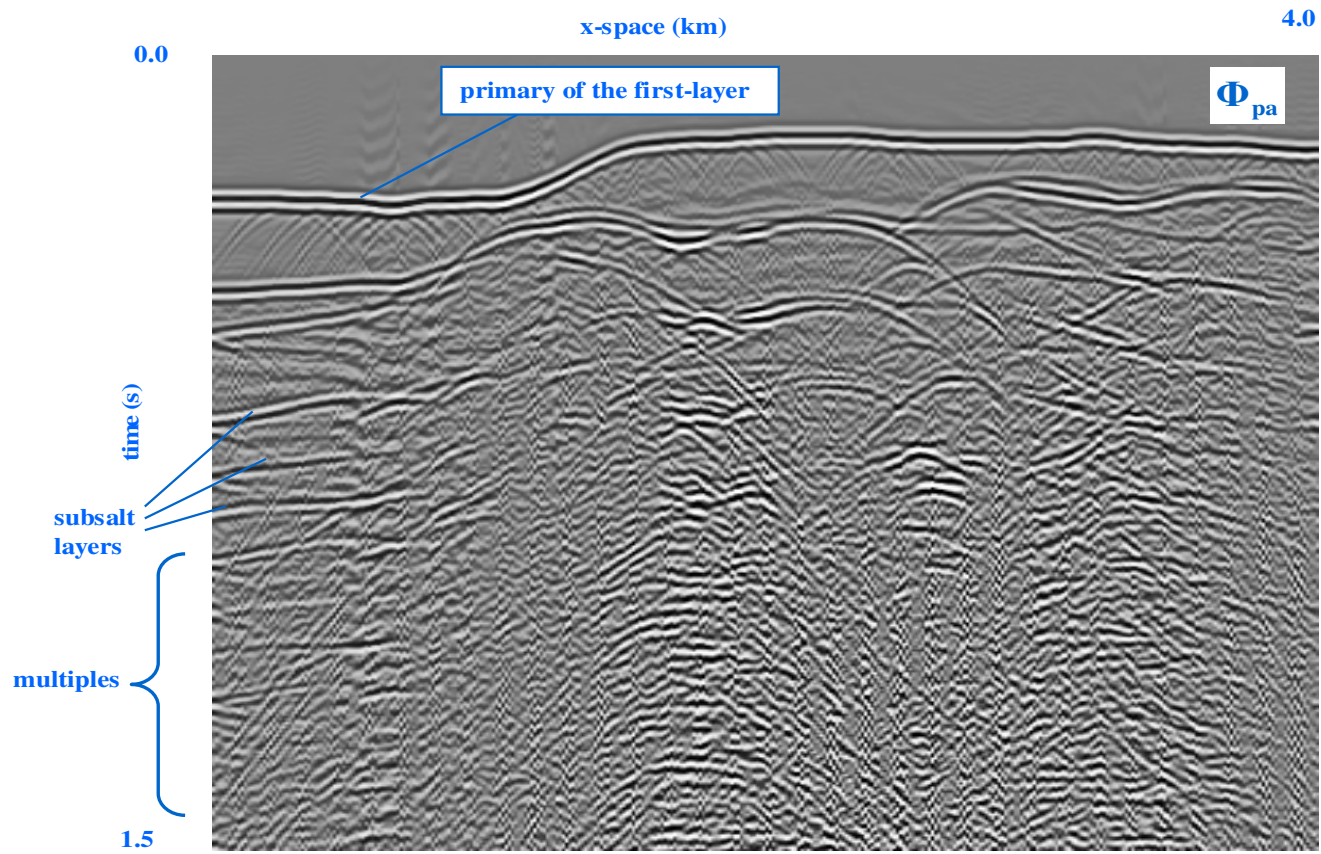


Figure 4.12: Zero offset data of the first demultiple result.

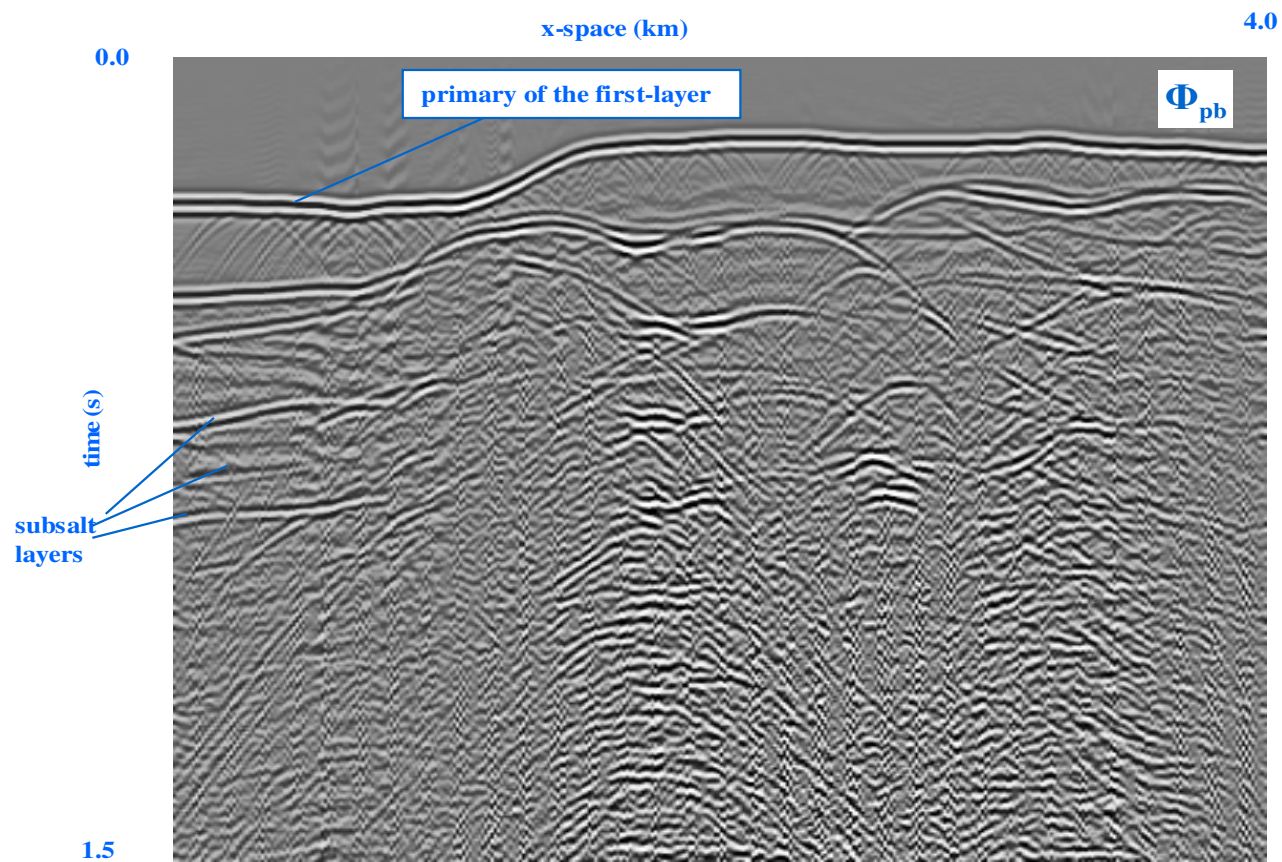


Figure 4.13: Zero offset data of the final demultiple result.

## Case II: Deep-Water Geology

The acquisition geometry and parameters for the deep-water depth environment are kept the same as for the shallow-water depth. See table 4.2 for a summary of the modeling parameters.

We applied the two steps of the BMG demultiple technique to the synthetic data. For our analysis, we consider the shots located at 500 m and 3000 m (see Figure 4.2 for shots locations). Shot located at 500 m represent the deepest water depth in our complex 2D geology. With this shot, we can demonstrate, that for the deep-water environment, where the BMG reflector is located deeper in the subsurface, the first step of the BMG demultiple technique is sufficient to attenuate free-surface multiples in the actual data. We have considered shot located at 3000 m to show that the weak primaries of the subsalt are preserved during the demultiple processes.

We start our analysis with the shot located at 500 m. Figure 4.14 is an example of  $\Phi_0$ , and an example of the portion of the data located above the BMG reflector  $V_0^a$  is Figure 4.15. Note that  $V_0^a$  is not small as compared to  $V_0^a$  in Figure 4.4 of our case I. We can therefore say our BMG reflector is not shallow.

An example of the field of the predicted free-surface multiples,  $\Phi_{1a}$ , is shown in Figure 4.16. By applying the first step of the demultiple technique, we obtained the first demultiple result  $\Phi_{pa}$  (Figure 4.17).

Note that free-surface multiples are still present in  $\Phi_{pa}$ . Therefore we still require the second step of the BMG demultiple technique to attenuate free-surface multiples.

The data below the BMG reflector  $V_{pa}^b$  is represented by Figure 4.18, and Figure 4.19 represents the field of predicted free-surface multiples  $\Phi_{1b}$ . Figure 4.20c is the final demultiple result  $\Phi_{pb}$ . Note that most of the free-surface multiples have been attenuated.



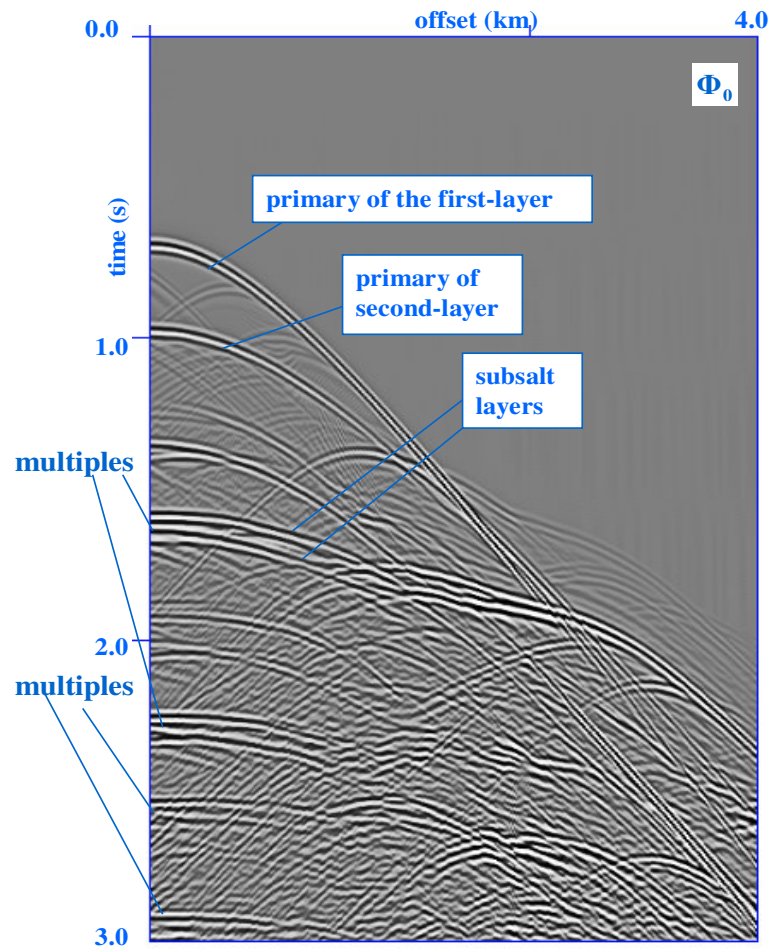


Figure 4.14: Shot gather of shot located at 500 m considered for the deep-water geology.

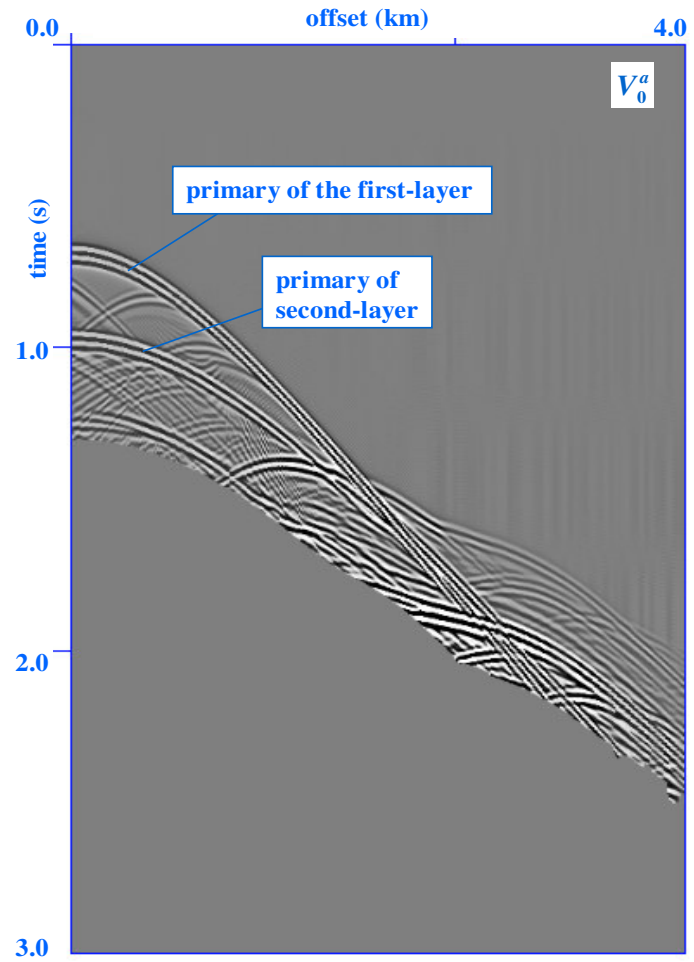


Figure 4.15: An example of data containing only primaries located above the BMG reflector.

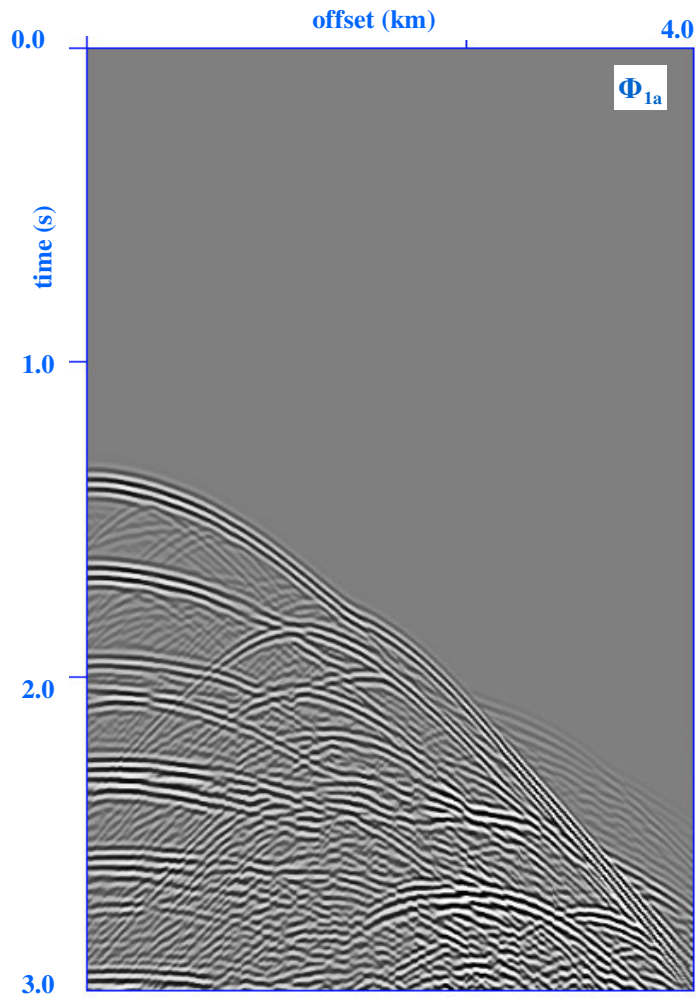


Figure 4.16: An example of the field of predicted free-surface multiples obtained from the multidimensional convolution of  $V_0^a$  with  $\Phi_0$ .

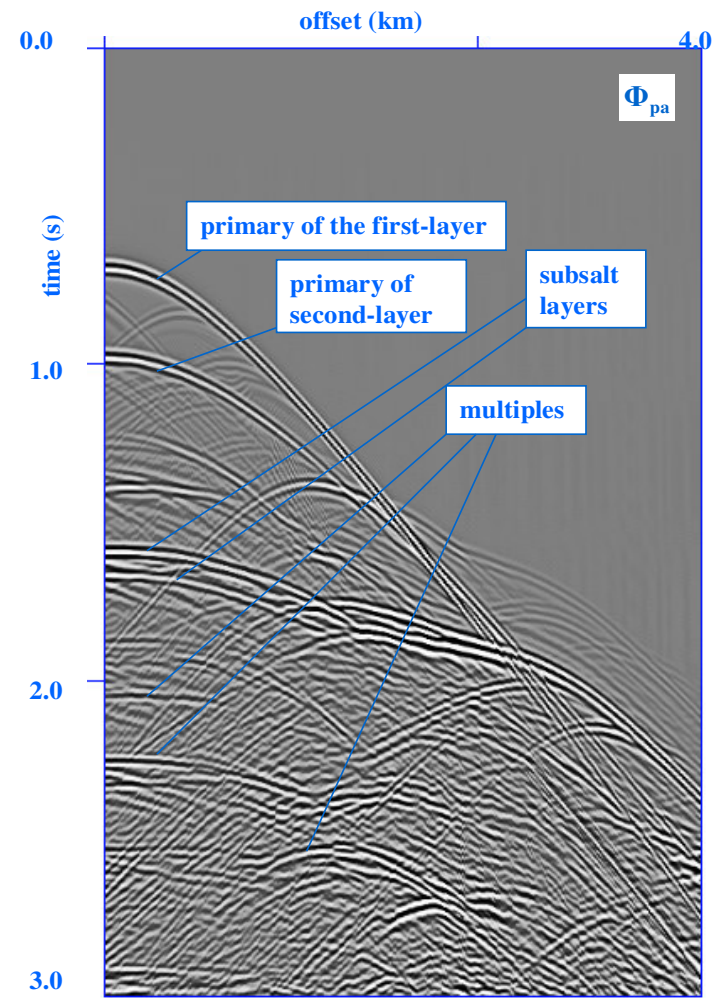


Figure 4.17: An example of the first demultiple result.

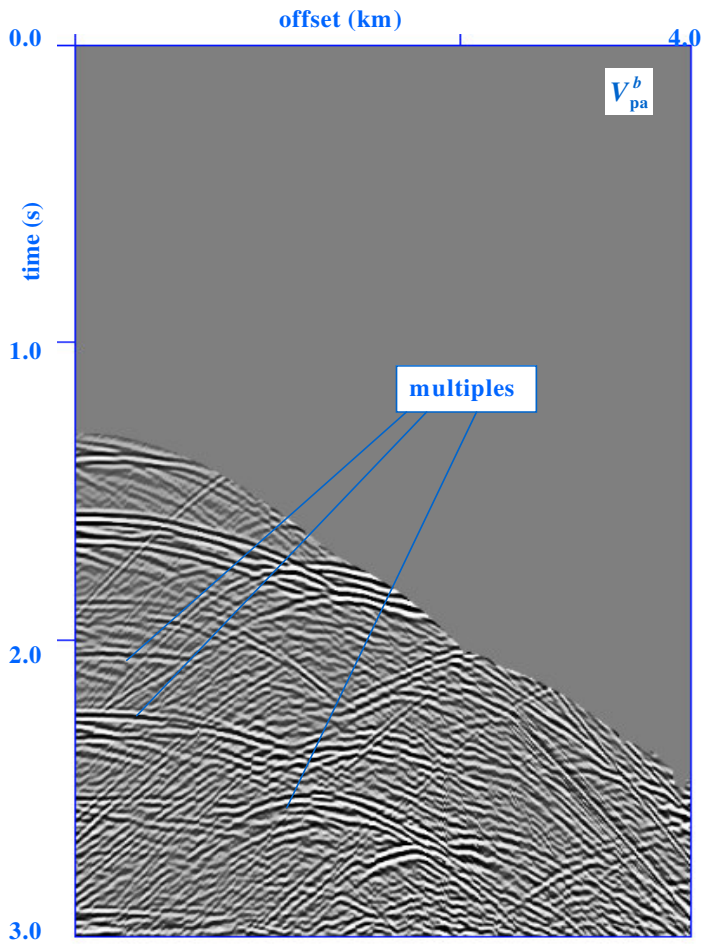


Figure 4.18: An example of the portion of data located below the BMG reflector.

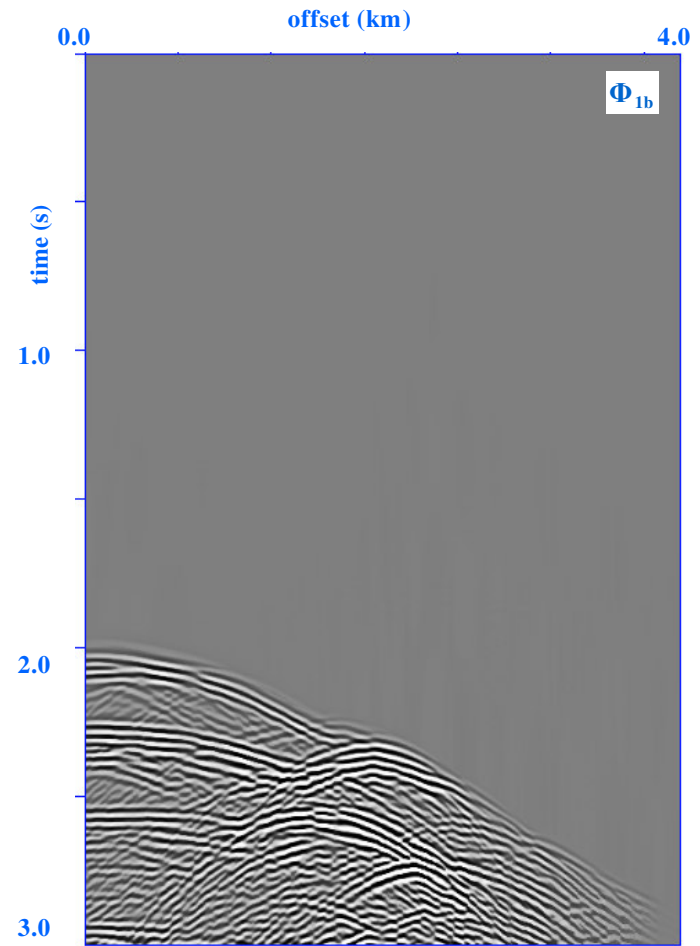


Figure 4.19: Shot gather showing the field of predicted free-surface multiples obtained from the multidimensional convolution of  $V_{pa}^b$  with  $\Phi_0^a$ .

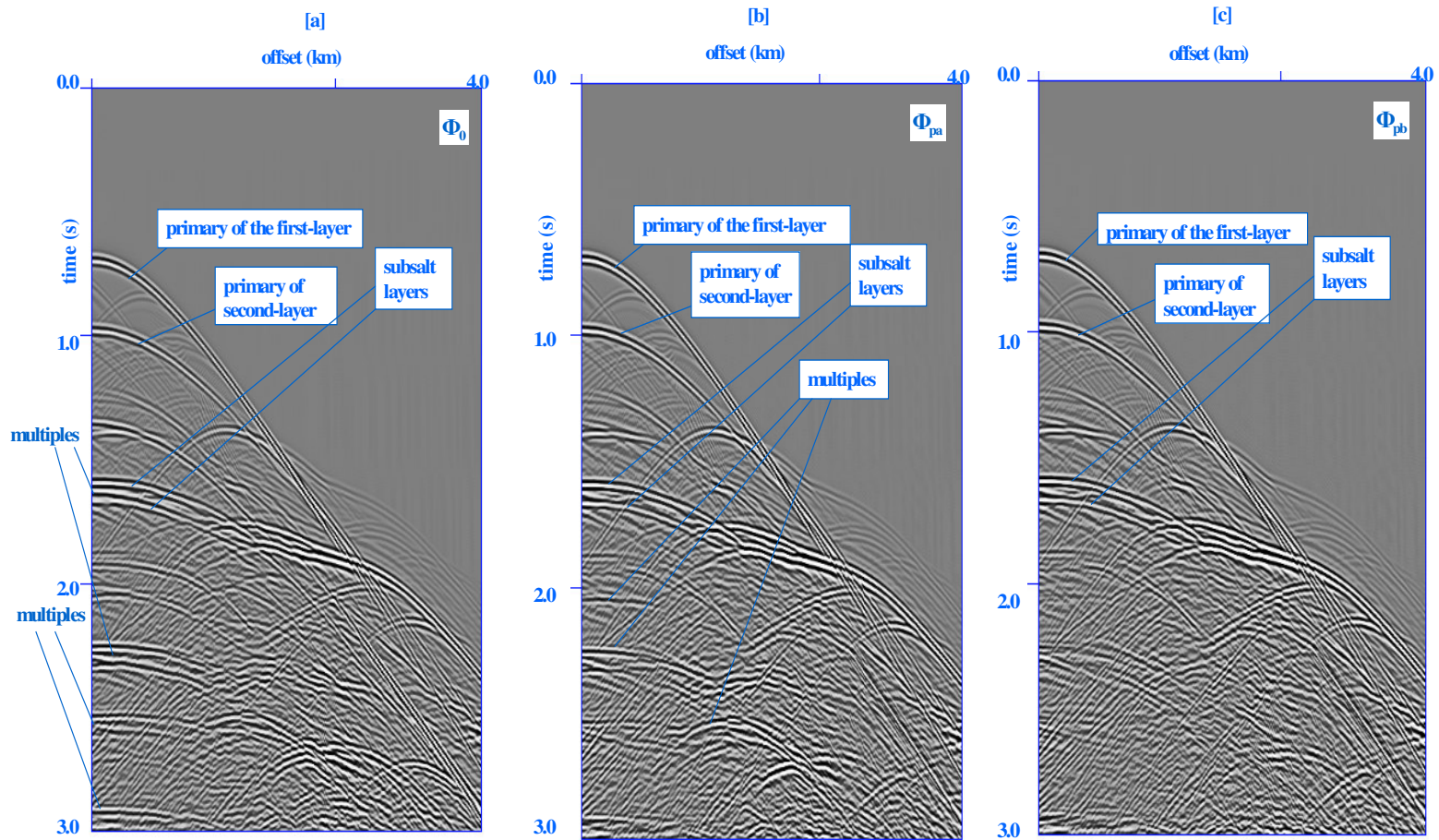


Figure 4.20 (a) An example of shot gather from the actual data (shot located at 500 m) before demultiple. (b) The first demultiple result (c) The second demultiple result.

We carried out another demonstration using the shot located at 3000 m. We follow the two steps of the BMG demultiple technique as applied in the previous demonstration, where Figure 4.21 shows the actual data  $\Phi_0$ , Figure 4.22 shows the portion the data containing only primaries located above the BMG reflector, Figure 4.23 shows an example of the field of predicted free-surface multiples and Figure 4.24 shows the first demultiple result  $\Phi_{pa}$ . Note that the subsalt layers has been preserved during the demultiple. Note also that the first step of the demultiple technique have effectively attenuated most of the free-surface multiples as compared to Figure 4.6. Although there are still presence of free-surface multiples residues in the data. Figure 4.25 is an example of the portion of the data below the BMG reflector, Figure 4.26 is an example of the field of predicted free-surface multiple, and Figure 4.27c shows the final demultiple result  $\Phi_{pb}$ . Notice that the residues have been well attenuated.

When we compared the demultiple results of the first step and the second step of the demultiple technique. Notice that the subsalt layers are preserved during the multiple attenuation processes and the weak subsalt layer, which could not be, define effectively in Figure 4.27a can be noticed.

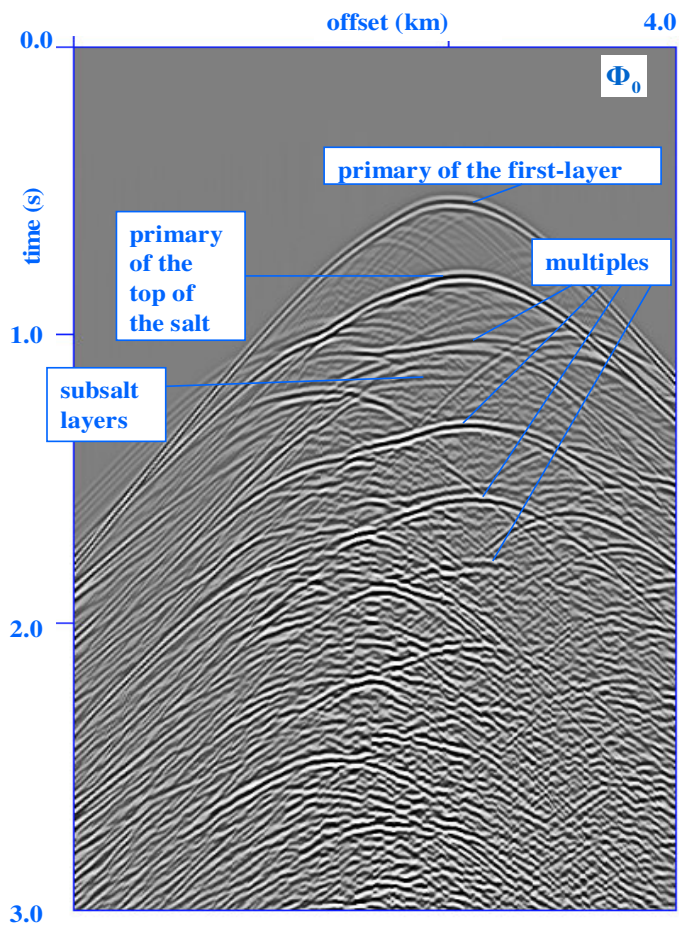


Figure 4.21: Shot gather of shot located at 3000 m considered for our analysis.

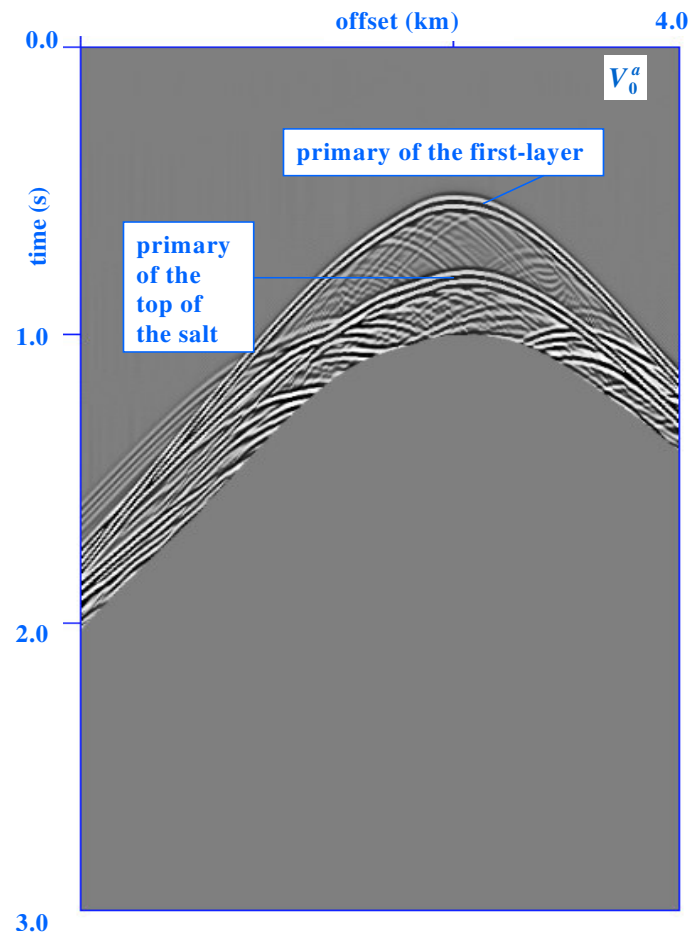


Figure 4.22: An example of the portion of the data containing only primaries located above the BMG reflector.

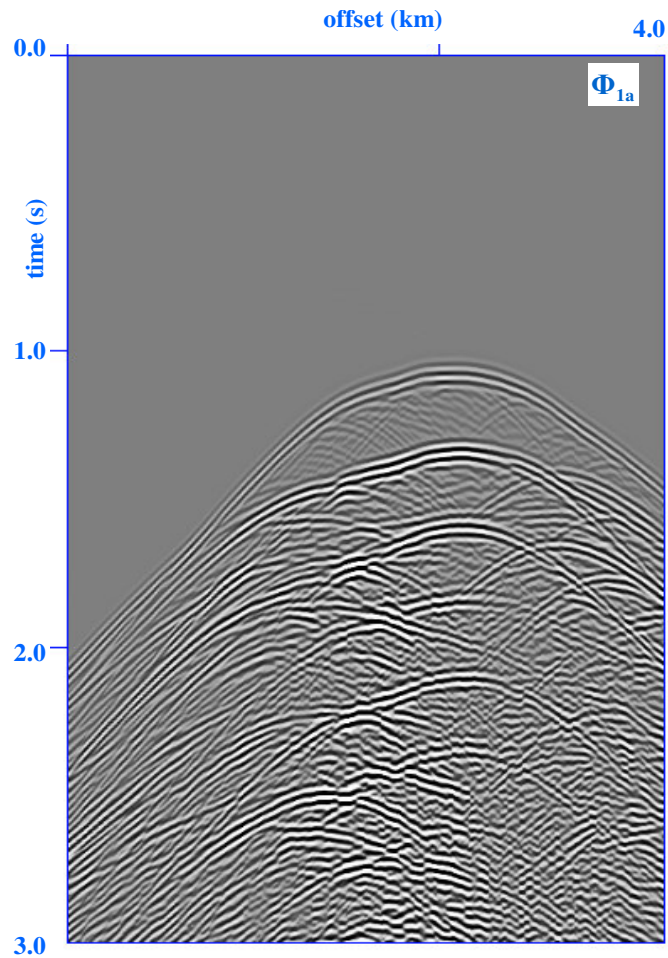


Figure 4.23: The field of predicted free-surface multiples obtained from the multidimensional convolution of  $V_0^a$  with  $\Phi_0$ .

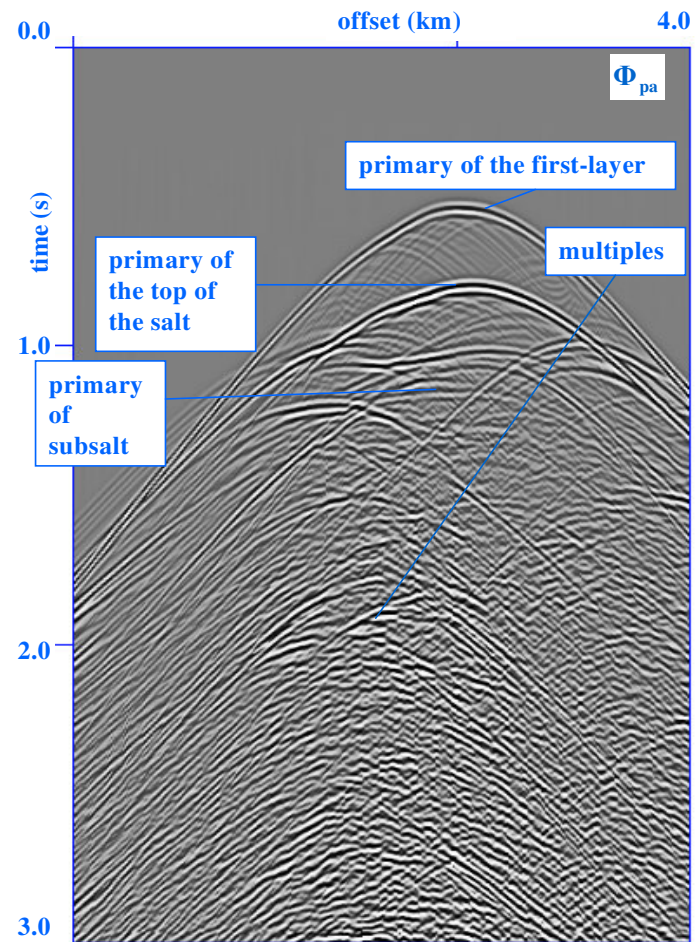


Figure 4.24: An example of the first demultiple result.

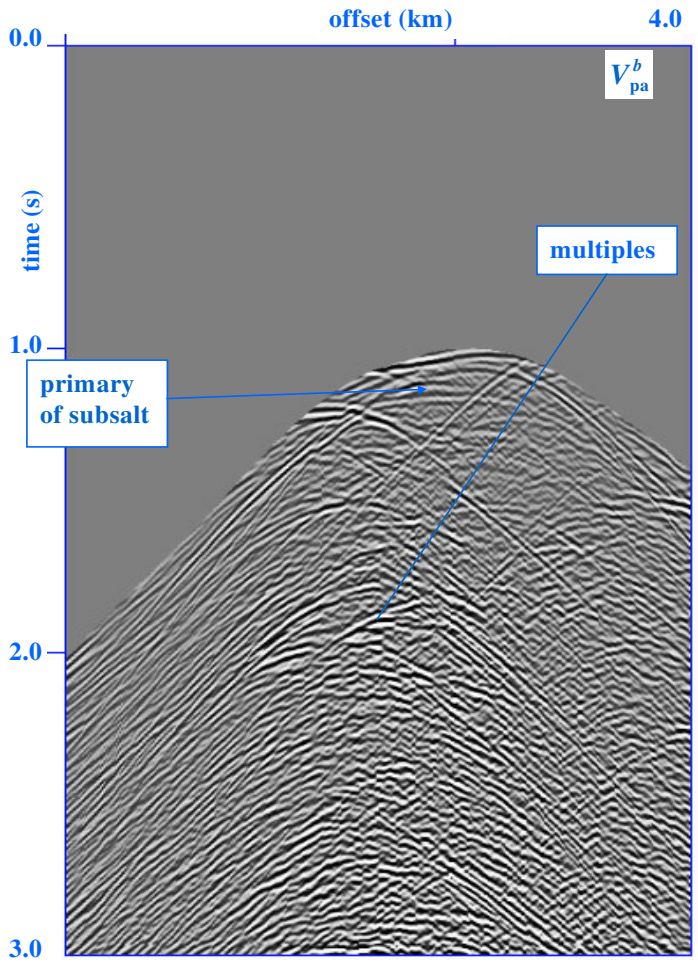


Figure 4.25: This is an example of the portion of  $\Phi_{pa}$  located below the BMG reflector.

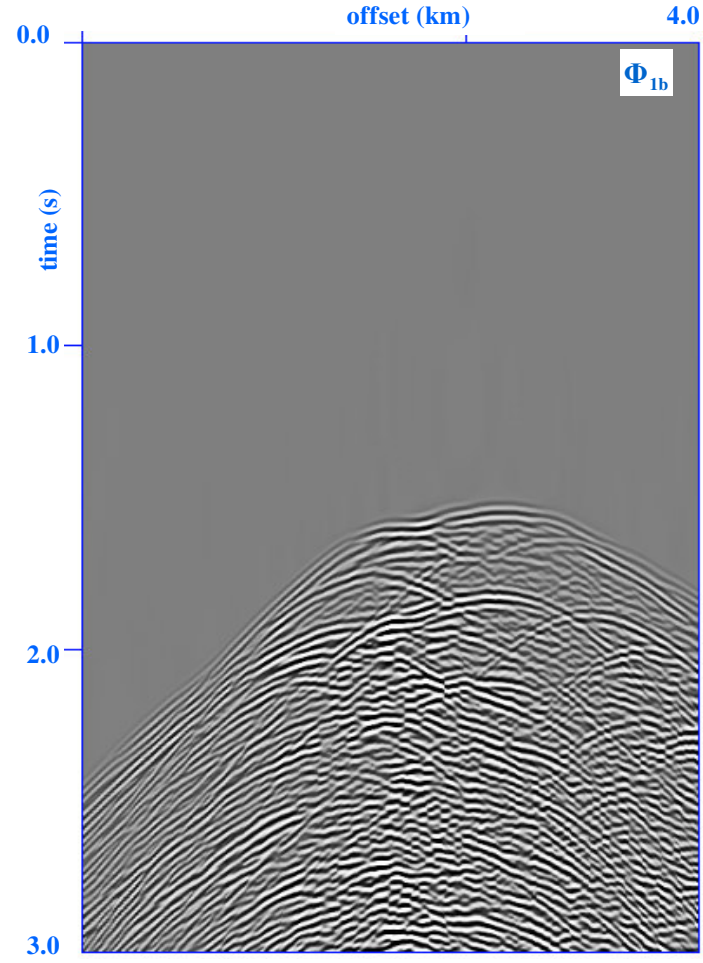


Figure 4.26: Shot gather showing an example of the field of predicted free-surface multiples obtained from the multidimensional convolution of  $V_{pa}^b$  with  $\Phi_0^a$ .



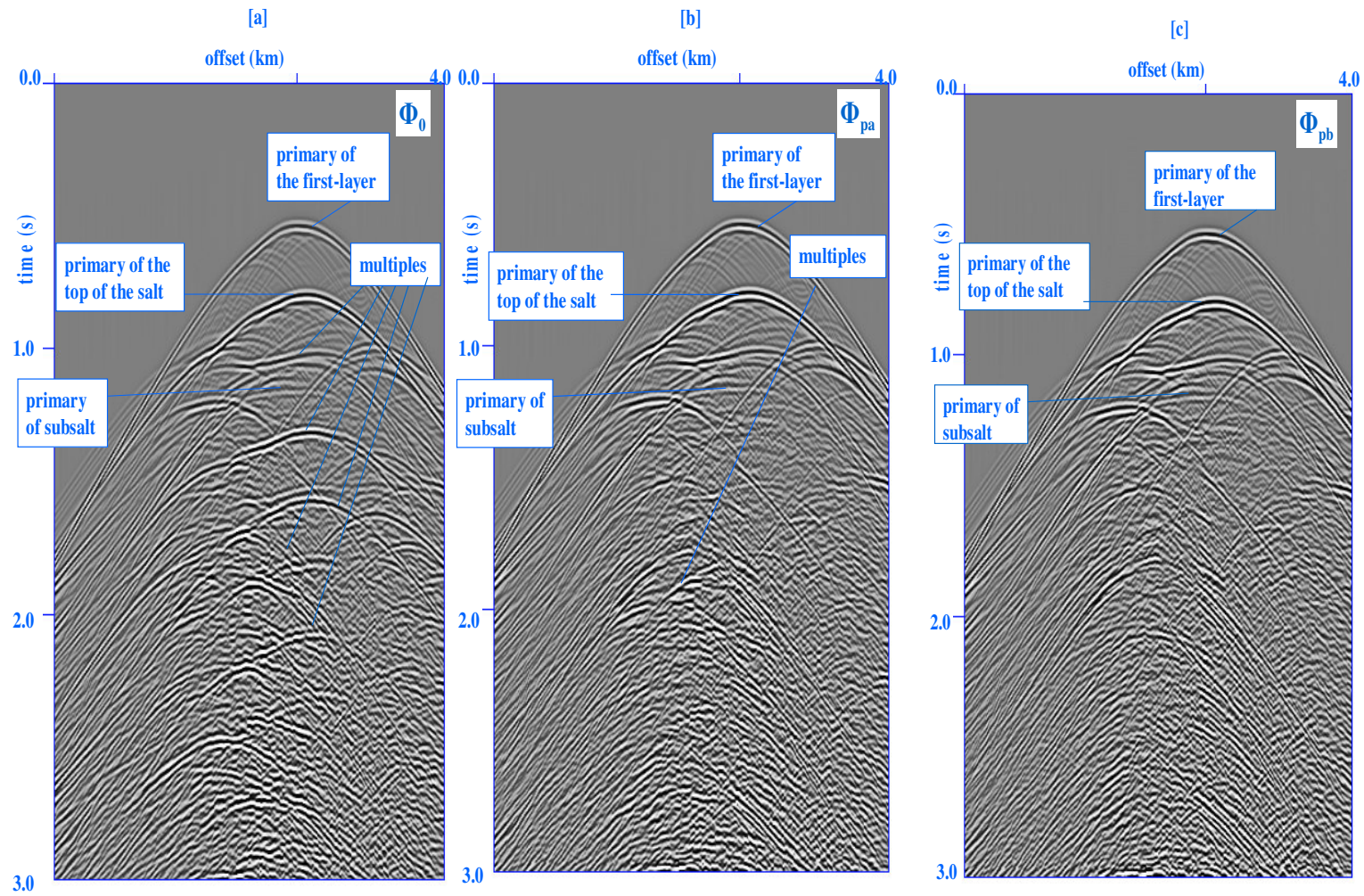


Figure 4.27: (a) An example of shot gather from the actual data (shot located at 3000 m) before demultiple. (b) The first demultiple result. (c) The second demultiple result.

Let us compare the zero offset data before and after the demultiple. Figure 4.28 show the zero offset data before the demultiple, while Figures 4.29 and 4.30 are the zero offset data of the first and second demultiple result. Note that by using the first step of the BMG demultiple technique, most of the free-surface multiples has been attenuated as compared to Figure 4.6, although there still residue of free-surface multiples that have not been attenuated by the application of the first demultiple technique.

Drawing from the results of the investigations, It can be noted that the first step of the BMG demultiple technique is not sufficient for free-surface multiple attenuation in deep-water environment. We still require the use of the second step to attenuate the free-surface multiples left in the seismic data.

Notice that the weak primary of the subsalt layers that was difficult to distinguished in Figure 4.28, are visible after the application of the first and second demultiple application. (Figures 4.29 and 4.30)

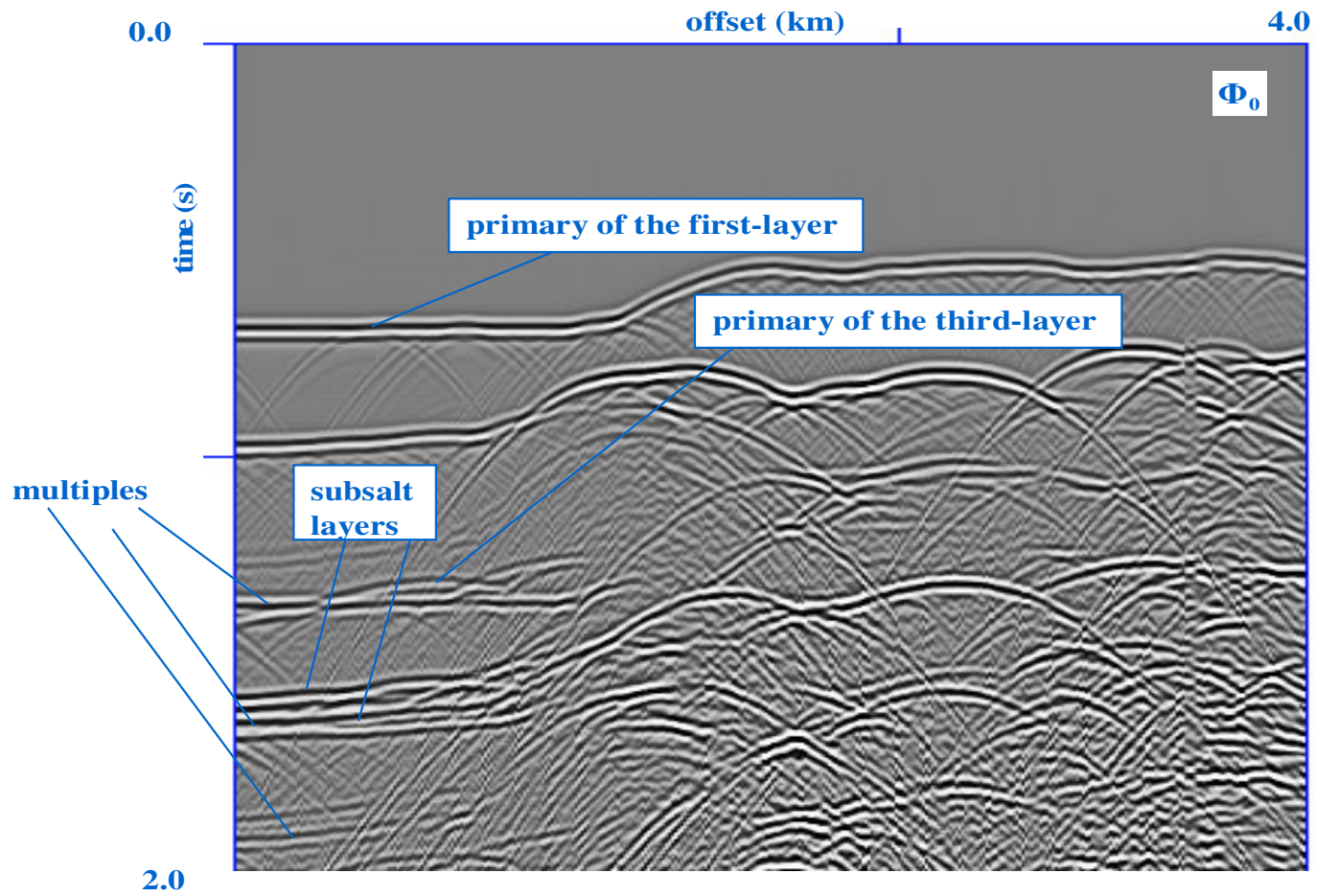


Figure 4.28: Zero offset of the synthetic towed-streamer data (deep-water geology) before demultiple.

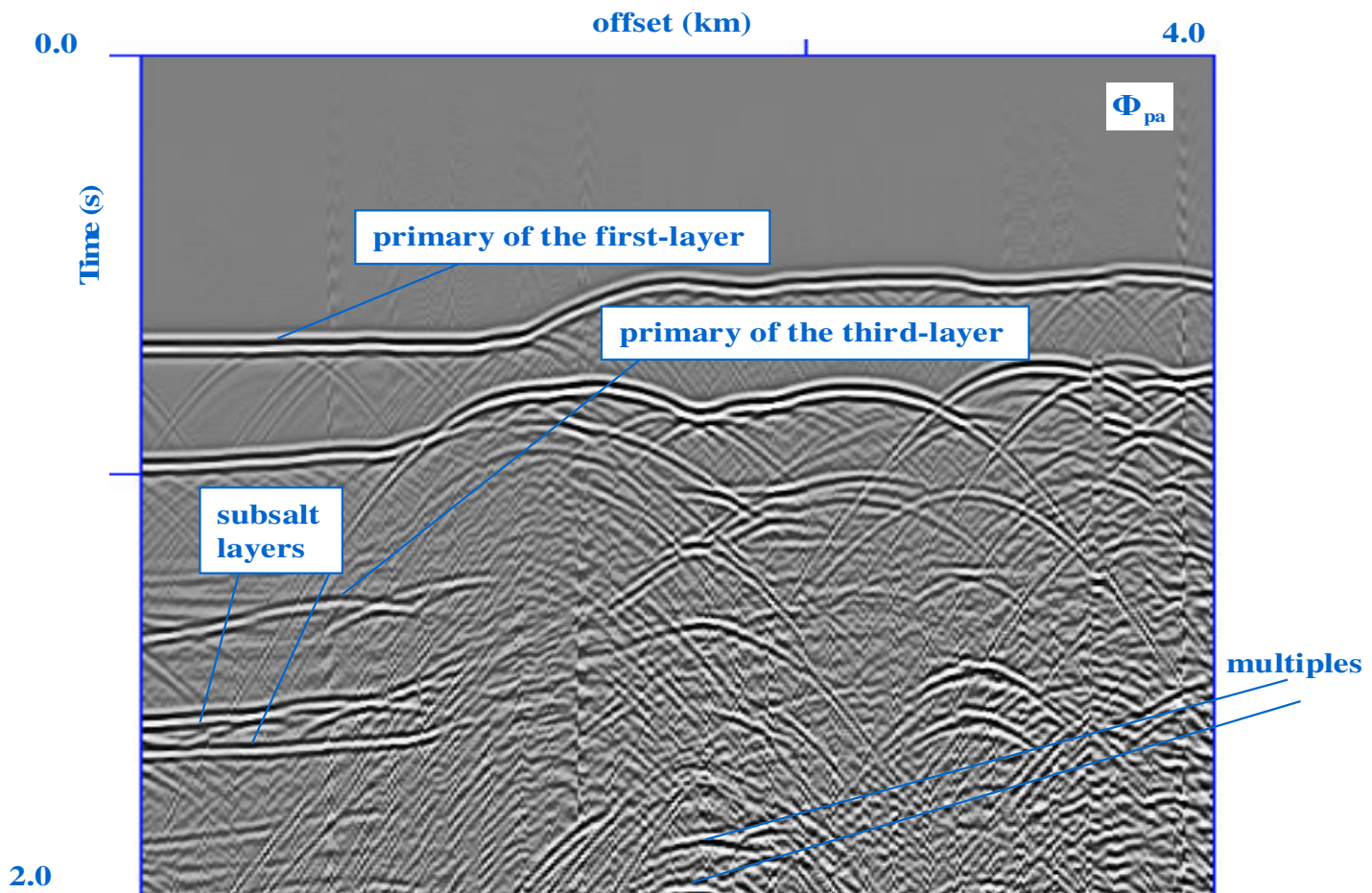


Figure 4.29: Zero offset of the synthetic towed-streamer data obtained after the first demultiple step.

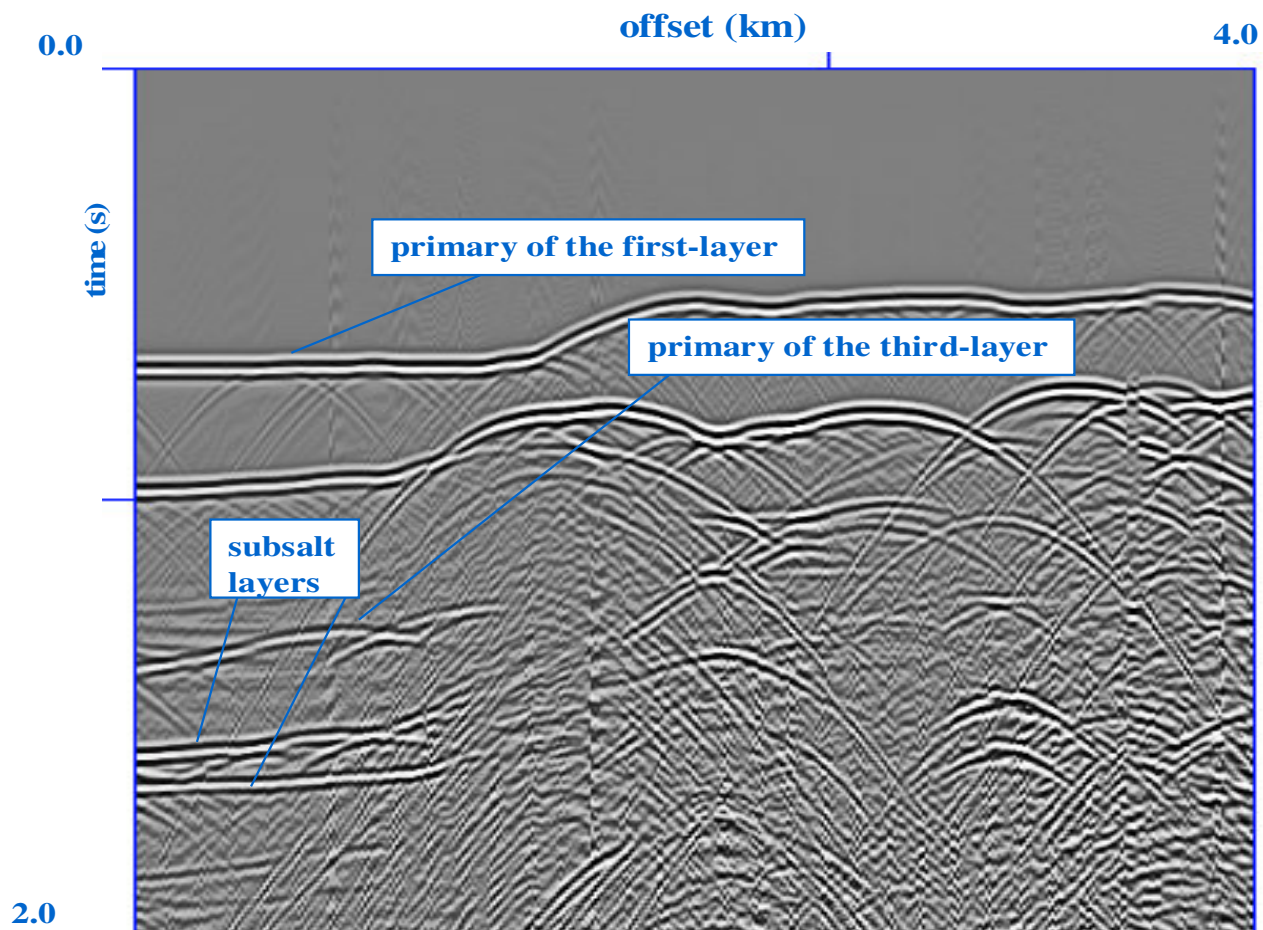


Figure 4.30: Zero offset of the synthetic towed-streamer data obtained after the second demultiple step

## CHAPTER V

### SUMMARY AND CONCLUSIONS

We have been able to show numerically that the BMG demultiple technique is not sensitive to how the mute at the BMG location is applied. In the shallow-water geology, the mute at the BMG cuts up some primaries but in the final demultiple result, free-surface multiples are attenuated while the primaries cut up by the mute are preserved. We also note that at both the near and far offsets, free-surface multiple attenuation was effective. Based on results obtained from our investigation, we make the conclusion that the BMG demultiple technique is effective in complex geology and does not fail either at near or far offsets.

We also demonstrated that the first step of the BMG demultiple may not be sufficient to attenuate free-surface multiples in a deep offshore environment. The second step of the BMG demultiple technique is required for us to obtain a data without free-surface multiples.

We have also shown that the weak subsalt primaries are preserved during the BMG demultiple technique application.

Our general conclusion is that the BMG demultiple technique is much more effective compared to other demultiple techniques. Another important conclusion is that there is savings in computation cost because the computation of the predicted free-surface multiples involves only two step.

Hence we recommend that the demultiple technique be incorporated as a preprocessing step in data processing.

## REFERENCES

- Ikelle, L. T., & Amundsen, L., 1997, Multiple attenuation at primary/multiple interferences: The Troll example: The Leading Edge, **16**, 1751-1753.
- Ikelle, L. T., Roberts, G., & Weglein, A. B., 1997, Source Signature Estimation Based on the Removal of First-Order Multiples: Geophysics, **62**, 1904-1920.
- Ikelle, L.T., & Amundsen, L., 2002, Noniterative multiple attenuation methods: Linear inverse solutions to nonlinear inverse problems: The Leading Edge, **21**, 350-356.
- Ikelle, L.T., & Amundsen, L., 2003, Introduction to petroleum seismology: Society of Exploration Geophysicists, Tulsa, OK, in press.
- Ikelle, L.T., & Amundsen, L., 2004, Attenuation of primaries and free-surface multiples of towed-streamer data while preserving ghosts of primaries: a linear approach: Journal of Seismic Exploration **13**, 1-15.
- Ikelle, L.T., Osen, A., Amundsen, L. & Shen, Y., 2004, Non-iterative multiple attenuation methods: linear inverse solutions to non-linear problems – II. BMG Approximation: Geophysical Journal International, **159**, 923-930.
- Lafond, J.I., Bridson, M., Houllévigie, H., Kerdran, Y., & Peliganga, J., 2004 Challenges in deep offshore imaging: West Africa. Canadian Society of Exploration Geophysicists, National Convention.
- Weglein, A. 1999, Multiple attenuation: an overview of recent advances and the road ahead: The Leading Edge, **18**, 40-43.



Yilmaz, O., 1987, Seismic data processing series: Society of Exploration Geophysicists, Tulsa, OK.

**APPENDIX A****LINEAR DEMULTIPLE SOLUTION BASED ON THE CONCEPT OF BOTTOM  
MULTIPLE GENERATOR (BMG) APPROXIMATION: SOME NEW RESULTS**

Abiola O. Watts and Luc T. Ikelle

CASP Project, Department of Geology and Geophysics

Texas A&M University, College Station, Texas 77843-3115 USA

**ABSTRACT**

The recent advances in demultiple have shown that a multidimensional convolution of a portion of data containing only primaries with the whole data (containing both primaries and multiples) can allow us to predict and attenuate all orders of free-surface multiples that are relevant for practical purposes. One way of constructing the portion of the data containing only primaries is by muting the actual data just above the first free-surface multiple to arrive. The location of the mute is generally known as the bottom multiple generator (BMG) reflector. The outstanding question about this method is how effective the technique can be when the BMG cuts through several seismic events, as the case in long offset data or in very complex shallow geology. In this paper, we present new results, which show the fact that the BMG may cut through several seismic events, this does not affect the accuracy or the cost of demultiple.

## INTRODUCTION

In the paper published by Ikelle et al (2004), a demultiple technique was proposed. The concept of the technique is to define a portion of the data containing only primaries by muting the data just above the first free-surface multiple to arrive. The location of the mute is also known as the bottom multiple generator (BMG) reflector. The multidimensional convolution of the portion of the data containing primaries with the actual data allows us to predict and attenuate all orders of free-surface multiples and therefore solve the problem of demultiple in towed-streamer data. The outstanding question not demonstrated by the examples presented in the paper, is what happens to demultiple results when the muting at the BMG reflector cuts through several seismic events.

In this paper, we demonstrated that this demultiple technique is effective, when the BMG cuts through several seismic events, by applying the technique to a synthetic dataset generated from a complex shallow geology (see Figure 1) using the elastic finite-difference modeling technique. Before we go into the details of our demonstration, let us first review the demultiple technique as described by Ikelle et al (2004).

The demultiple technique can be described as a two-step process. Let us denote the two components of towed-streamer data without the direct-wave arrivals by  $\Phi_0 = \{P_0, V_0\}$ , where  $P_0$  is the pressure data and  $V_0$  is the vertical particle velocity, and let us denote the portion of towed-streamer data above the BMG reflector as  $\Phi_0^a = \{P_0^a, V_0^a\}$ . Then the first step of the demultiple technique is given by

$$\Phi_{pa} = \Phi_0 + a\Phi_{1a} \quad (1)$$

The inverse source signature is denoted by  $a$ , and  $\Phi_{1a}$  is the multidimensional convolution of  $V_0^a$  by  $\Phi_0$ . See the illustration of events generated by the multidimensional convolution in Figure 2. Note that only free-surface multiples that have their first bounce in the subsurface above the BMG reflector are predicted and therefore attenuated. A second step is required to attenuate free-surface multiples that are still present in  $\Phi_{pa}$ .

Let us denote  $V_{pa}^b$  as a portion of  $V_{pa}$  ( $V_{pa}$  is a component of  $\Phi_{pa}$  corresponding to the particle velocity) located below the BMG reflector. The second step is given below as

$$\Phi_{pb} = \Phi_{pa} + a\Phi_{1b}, \quad (2)$$

where  $\Phi_{1b}$  is the multidimensional convolution of  $V_{pa}^b$  by  $\Phi_0^a$ . Figure 3 shows the illustration of events generated by the multidimensional convolution. Noticed that the second step does not predict free-surface multiples whose first and last bounces in the subsurface are below the BMG reflector (see the scattering diagram illustrating these types of free-surface multiples in Figure 4). These types of free-surface multiples are usually weak in deep water and therefore as negligible as internal multiples.

Now that we have reviewed the Ikelle et al (2004) demultiple technique, let us go

back and show that the technique will work even when the muting at the BMG reflector cuts through several seismic events of our synthetic data.

### **APPLICATION OF THE BMG DEMULTIPLE TECHNIQUE**

Let us examine the synthetic towed-streamer data used for our application, which we generated using the elastic finite-difference modeling technique. Figure 1 shows the 2D geological model considered for our application. We have designed our geological model to have a shallow water depth and irregular salt bodies that are located close to the sea-floor. We designed our model this way in order, to generate primaries that are needed to predict multiples and to have their trajectories cross the BMG location. Our objective in this paper is to show the effectiveness of the BMG-based demultiple technique even in this kind of situation. So, we have generated 321 shots from 500 m to 4500 m (source depth is at 5 m) and spaced at 12.5 m each. The number of receivers used is 321, which are also placed from 500 m to 4500 m (receiver depth is at 10 m) and spaced at 12.5 m apart.

We have based our analysis on a shot located at 500 m (Figure 1 shows the location of the shot on the geological model while Figure 5a shows a shot gather of the shot). We have considered this shot because it is a good representation of all offsets and events that pass through the salt bodies.

Let us demonstrate the demultiple steps described in our introduction. We first defined the portion of the data containing only primaries  $V_0^a$  by muting the data at the BMG location. An example of  $V_0^a$  is shown in Figure 5b. We muted the data at the

BMG location by taking a small portion of the actual data  $\Phi_0$  and performed the autoconvolution of this small portion to produce a portion of  $\Phi_1$  containing the first multiples that we needed to define the BMG location. Note that from the example shown in Figure 5b,  $V_0^a$  is small when compared to the actual data (Figure 5a). Note also that the mute at the BMG location cuts up the primary of the top of the salt body.

Let us now examine multiples predicted by the multidimensional convolution of  $V_0^a$  with the actual data,  $\Phi_0$ . The result of the multidimensional convolution is denoted here as  $\Phi_{1a}$  (an example is shown in Figure 5c). The multiples contained in  $\Phi_{1a}$  are predicted free-surface multiples whose first bounce in the subsurface is located above the BMG reflector. Note that the multiple of the primary of the top salt that was cut-up at the BMG location in Figure 5b is not predicted fully. The next step is to apply equation (1) to attenuate multiples predicted in  $\Phi_{1a}$ . The demultiple result  $\Phi_{pa}$  after step one is shown in Figure 5d. Note that free-surface multiples, which are not predicted by,  $\Phi_{1a}$  are still present in  $\Phi_{pa}$ . We have applied the second step described in equation (2) of the demultiple technique to attenuate the remaining free-surface multiples.

We first compute the portion of the  $\Phi_{pa}$  below the BMG,  $V_{pa}^b$ . An example of  $V_{pa}^b$  is Figure 6a. The multidimensional convolution of  $V_{pa}^b$  with the portion of the actual data above the BMG reflector,  $\Phi_0^a$ , predicts  $\Phi_{1b}$  (Figure 6b). The multiples contained in  $\Phi_{1b}$  are free-surface multiples which have their first bounce below the BMG reflector. Note in Figure 6b that the other portion of the multiple associated with the cut-up

primary of the top of salt is predicted. Using equation (2), the final demultiple result  $\Phi_{pb}$  (Figure 6c) is obtained. Note in Figure 6c that the free-surface multiples interfering with primaries at about 0.7 s to 1.22 s have been completely attenuated.

It should be noted that the BMG should not be shallow, and if shallow, the BMG has to be lowered according to Ikelle et al (2004). For this demonstration we have made our BMG location shallow so that we can obtain primaries that severely overlap the BMG location. Free-surface multiples which are not modeled by  $\Phi_{1b}$  (see Figure 4 for these types of free-surface multiples) are visible because of the shallow BMG.

## CONCLUSION

We have demonstrated numerically that the BMG demultiple technique is effective and not sensitive to the way the mute at BMG location is applied. Even when the mute at the BMG cuts through several seismic events, it does not affect the demultiple result. Therefore we concluded that the BMG is applicable in both complex geology and long-offset data.

## ACKNOWLEDGMENTS

We would like to thank the sponsors of the CASP project for their comments and suggestions during the review process.

## REFERENCE

- Ikelle, L. T., and Amundsen, L., 2004, Attenuating primaries and free-surface multiples of towed-streamer data while preserving ghosts of primaries: a linear approach  
Journal of Seismic Exploration: **13**, 1-15.
- Ikelle, L. T., Osen, A., Amundsen, L., Shen, Y., 2004, Noniterative multiple-attenuation methods: linear inverse solutions to nonlinear inverse problems II -- BMG approximation: GJI, **159**, 923-930.
- Ikelle, L. T., and Amundsen, L., 1997, Multiple attenuation at primary/multiple interferences: The troll example: The Leading Edge, **16**, 1751-1753.
- Lafond, J. I., Bridson, M., Houllevigue, H., Kedran, Y., and Peliganga, J., 2004, Challenges in deep offshore imaging: West Africa. Canadian Society of Exploration Geophysicists, National Convention.

## FIGURE CAPTIONS

**Figure 1:** 2D geological model adapted from Lafond et al 2004. This is the model considered for the application of the BMG demultiple technique.

**Figure 2:** An illustration of the scattering diagram of free-surface multiples predicted by the multidimensional convolution of  $V_0^a$  by  $\Phi_0$ . These predicted free-surface multiples are attenuated using equation (1).

**Figure 3:** An illustration of the scattering diagram of free-surface multiples predicted by the multidimensional convolution of  $V_{pa}^b$  by  $\Phi_0^a$ . These predicted free-surface multiples are attenuated using equation (2). Note that free-surface multiples that



have their first and last bounces below the BMG reflector are not predicted.

**Figure 4:** An illustration of the scattering diagram of free-surface multiples that have their first and last bounces below the BMG reflector and are not predicted in the two demultiple steps.

**Figure 5:** (a) Shot gather of the shot located at 500 m generated off the geological in Figure 1 (This is an example of the actual data  $\Phi_0$ . Notice that free-surface multiples interfere with primaries at about 0.7 s to 1.22 s. (b) An example of  $V_0^a$  (the portion of the particle velocity of the data containing only primaries located above the BMG reflector). Notice that the mute at the BMG cut up primary of the top of salt. (c) An example of predicted multiples  $\Phi_{1a}$ . Notice that the multiple of the primary of the top of salt cut up at the BMG is not predicted fully. (d) The result of the demultiple after applying equation (1). Note that Figure 5d contains some free-surface multiples, which are not predicted by  $\Phi_{1a}$ . We applied the second step of the demultiple technique described in equation (2) to attenuate these free-surface multiples.

**Figure 6:** (a) An example of  $V_{pa}^b$  (the portion of the particle velocity of  $\Phi_{pa}$  located below the BMG reflector). (b) An example of predicted free-surface multiples  $\Phi_{1b}$ . Notice that the other portion of the multiple of the primary of the top of salt cut up at the BMG is predicted. (c) The final demultiple result obtained after applying equation (2). Notice that most of the free-surface multiples that interfere with the primaries at about 0.7 s to 1.22 s have been attenuated. The free-surface multiples still present in the

final demultiple result are those not predicted in both steps of the demultiple technique. (Figure 4 shows an illustration of these types of free-surface multiples.) Note that because we have made our water depth shallow for this demonstration of the BMG demultiple technique, the leftover multiples are visible. Ideally in deep water, which is usually the case in marine acquisition, these multiples will appear weak and therefore negligible.

## FIGURES

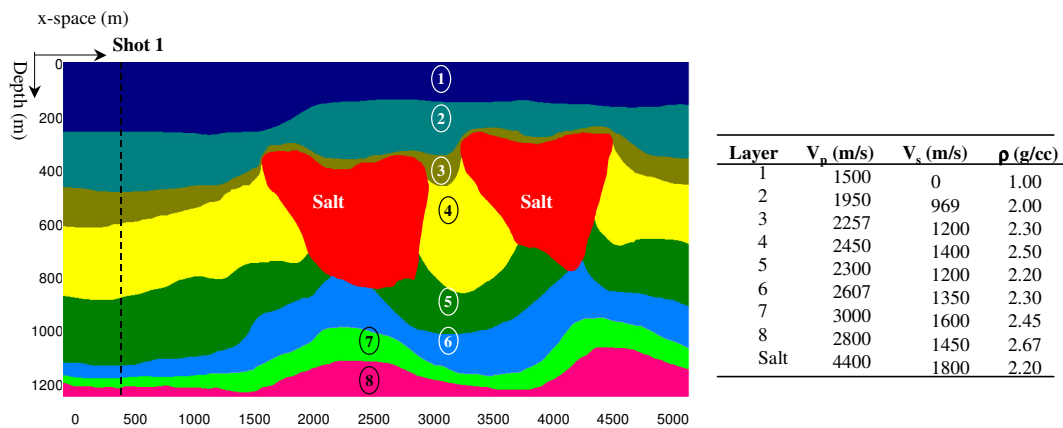


**Figure 1:** 2D geological model adapted from Lafond et al. (2004). This is the model considered for the BMG demultiple application.

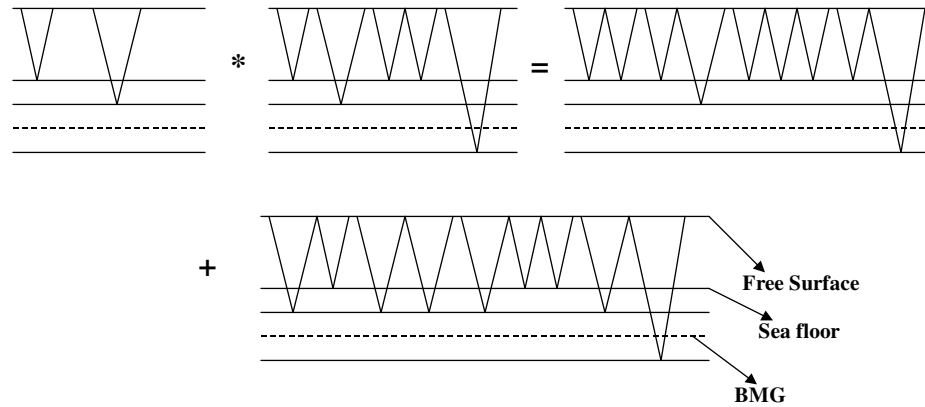


**Figure 2:** An illustration of the scattering diagram of free-surface multiples predicted by the multidimensional convolution of  $V_0^a$  by  $\Phi_0$ . These predicted free-surface multiples are attenuated using Equation (1).

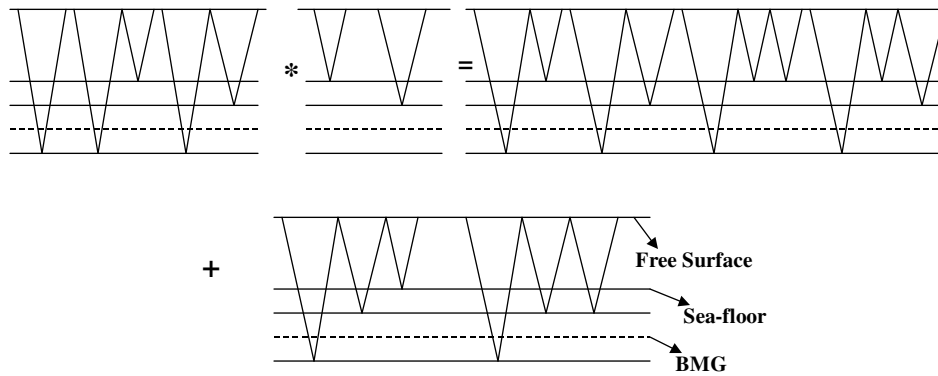


**Figure 3:** An illustration of the scattering diagram of free-surface multiples predicted by the multidimensional convolution of  $V_{pa}^b$  by  $\Phi_0^a$ . These predicted free-surface multiples are attenuated using Equation (2). Note that free-surface multiples that have their first and last bounces below the BMG reflector are not predicted.

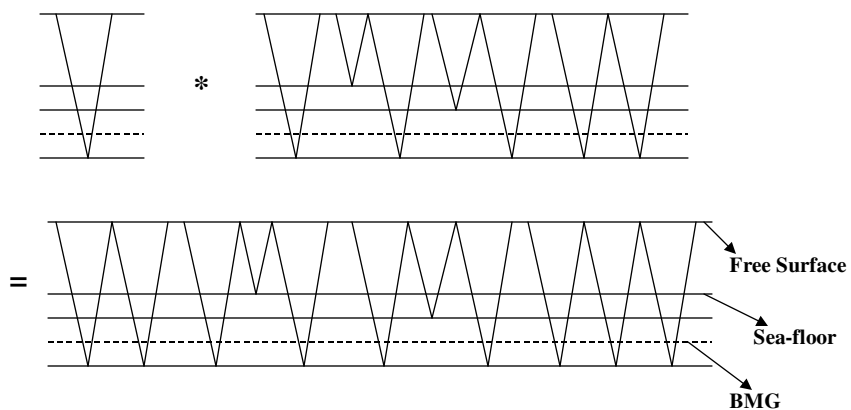


**Figure 4:** An illustration of the scattering diagram of free-surface multiples that have their first and last bounces below the BMG reflector and are not predicted in the two demultiple steps.

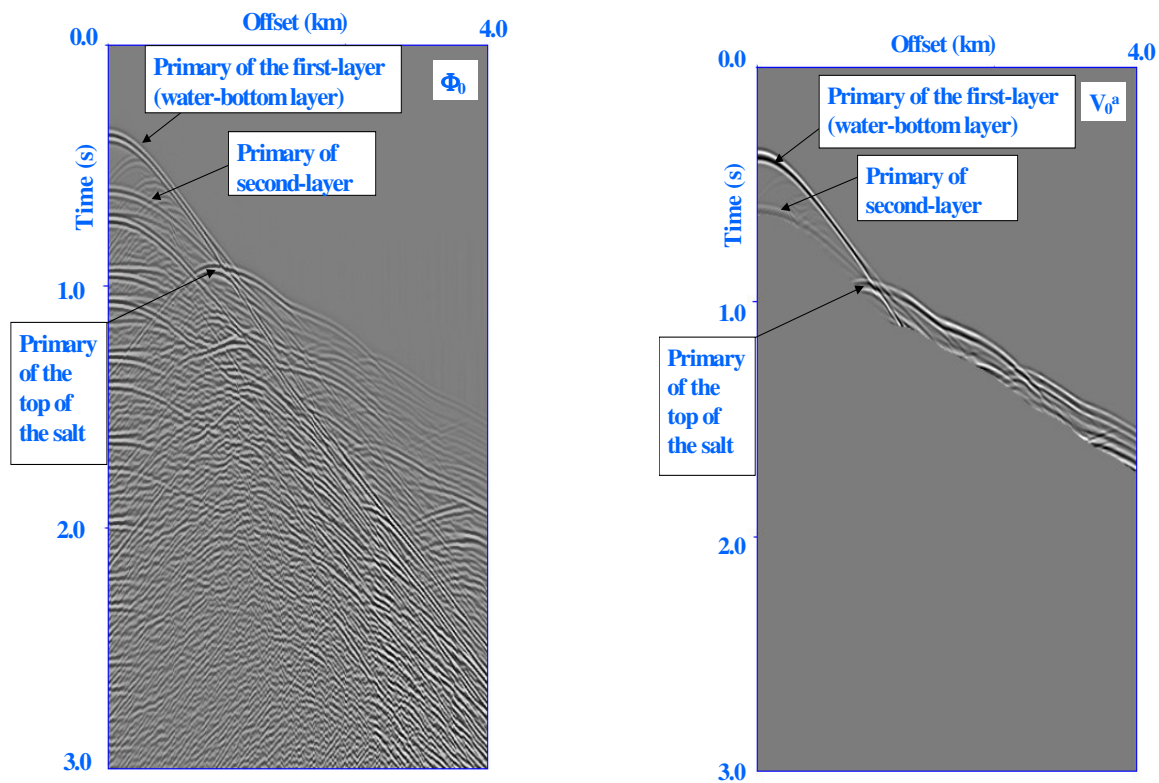


**Figure 4:** (a) Shot gather of the shot located at 500 m (an example of  $\Phi_0$ ). Notice that free-surface multiples interfere with primaries at about 0.7 s to 1.22 s. (b) An example of the portion of the particle velocity of the data containing only primaries located above the BMG reflector. Notice that the mute at the BMG cut up primary of the top of salt.

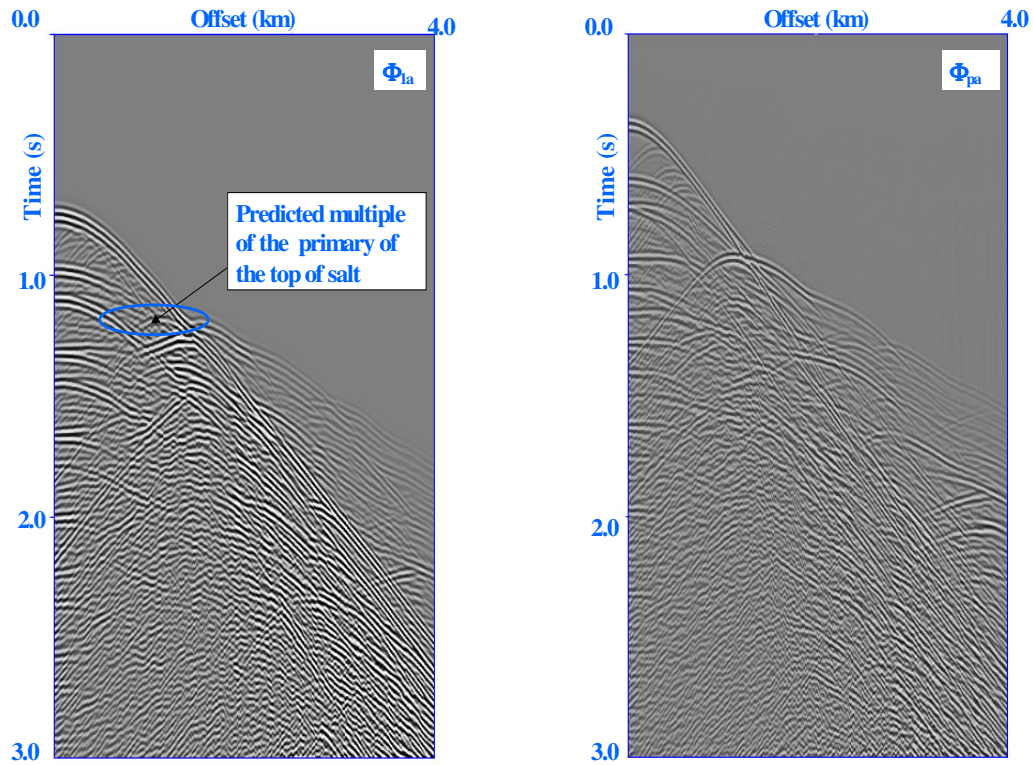


**Figure 4:** (c) An example of predicted multiples,  $\Phi_{1a}$ . Notice that the multiple of the primary of the top of salt cut up at the BMG is not predicted fully. (d) The result of the demultiple after applying Equation (1). Note that Figure 4d contains some free-surface multiples, which are not predicted by  $\Phi_{1a}$ . We applied the second step of the demultiple technique described in Equation (2) to attenuate these free-surface multiples.

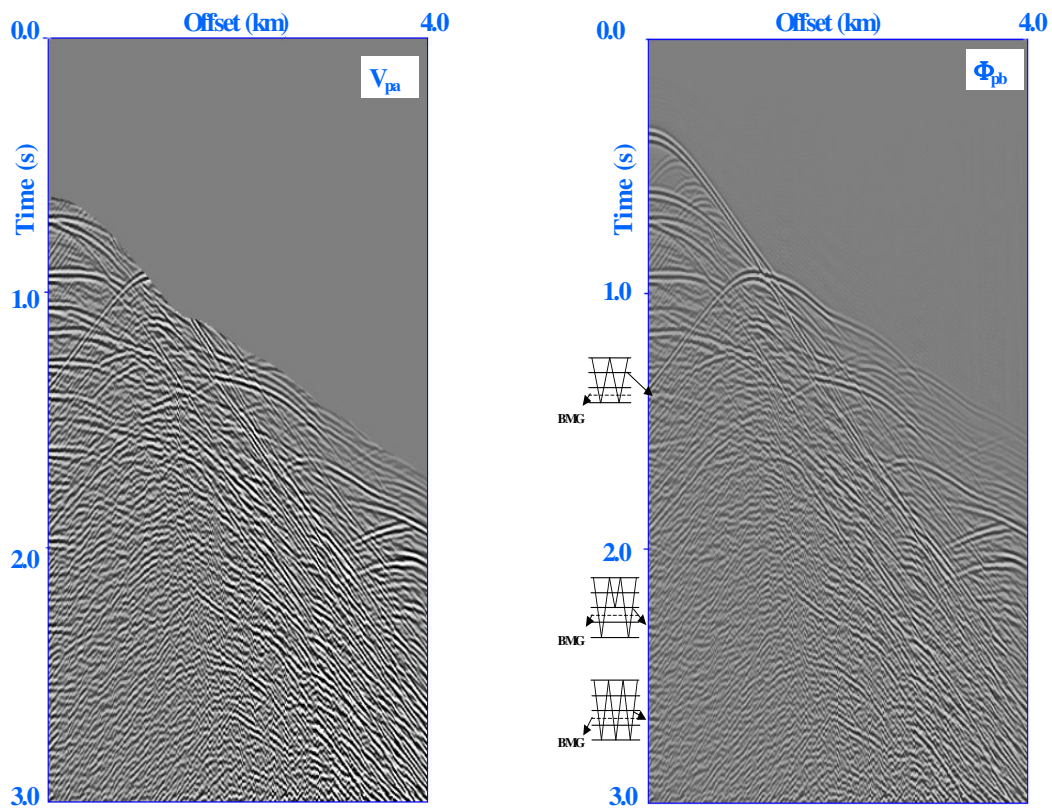


**Figure 4:** (e) An example of the portion of the particle velocity of  $\Phi_{pa}$  located below the BMG reflector. (f) The final demultiple result obtained after applying Equation (2). Notice that most of the free-surface multiples that interfere with the primaries at about 0.7 s to 1.22 s have been

## APPENDIX B

### A REVIEW OF FINITE DIFFERENCE MODELING

In this research, we used the finite difference modeling (FDM) technique to generate the synthetic data used for demultiple investigation. We review the explicit approach to finite difference as described in Appendix C of Ikelle and Amundsen (2003).

#### Basic Equations for Elastodynamic Wave Motion in Elastic Media

The equations of momentum conservation are

$$\rho(\mathbf{x})\partial_t v_x(\mathbf{x}, t) - \{\partial_x \tau_{xx} + \partial_z \tau_{zx}(\mathbf{x}, t)\} = f_x(\mathbf{x}, t) \quad (1)$$

$$\rho(\mathbf{x})\partial_t v_z(\mathbf{x}, t) - \{\partial_x \tau_{xz} + \partial_z \tau_{zz}(\mathbf{x}, t)\} = f_z(\mathbf{x}, t) \quad (2)$$

where the component of the particle velocity is denoted as  $\mathbf{v} = (v_x, v_z)$ ,  $\boldsymbol{\tau} = \tau_{xx}, \tau_{zz}, \tau_{xz}$  denotes the stress components and  $\mathbf{f} = (f_x, f_z)$  denotes the components of the body force.

The stress-strain relations for an isotropic elastic medium are as follows:

$$\partial_t \tau_{xx}(\mathbf{x}, t) = [\lambda(\mathbf{x}) + \mu(\mathbf{x})]\partial_x v_x(\mathbf{x}, t) + \lambda(\mathbf{x})\partial_z v_z(\mathbf{x}, t) + I_{xx}(\mathbf{x}, t) \quad (3)$$

$$\partial_t \tau_{zz}(\mathbf{x}, t) = [\lambda(\mathbf{x}) + \mu(\mathbf{x})]\partial_z v_z(\mathbf{x}, t) + \lambda(\mathbf{x})\partial_x v_x(\mathbf{x}, t) + I_{zz}(\mathbf{x}, t) \quad (4)$$

$$\partial_t \tau_{xz}(\mathbf{x}, t) = \mu(\mathbf{x})[\partial_z v_x(\mathbf{x}, t) + \lambda(\mathbf{x})\partial_x v_z(\mathbf{x}, t)] + I_{xz}(\mathbf{x}, t) \quad (5)$$

where  $\mathbf{I} = (I_{xx}, I_{zz}, I_{xz})$  denotes the components of the stress force. The wave motion satisfies a set of first-order coupled differential equations, equations (1)-(5). This set of



first-order coupled equations differential equations can be formulated into second-order differential equations for stress and particle velocity. For particle velocity the second-order differential equations are as follows:

$$\begin{aligned} \rho(\mathbf{x})\partial_t^2 v_x(\mathbf{x},t) - \partial_x [\lambda(\mathbf{x})(\partial_x v_x(\mathbf{x},t) + \partial_z v_z(\mathbf{x},t)) + 2\mu(\mathbf{x})\partial_x v_x(\mathbf{x},t)] \\ + \partial_z [\mu(\mathbf{x})(\partial_x v_z + \partial_z v_x)] = F_x(\mathbf{x},t) \end{aligned} \quad (6)$$

$$\begin{aligned} \rho(\mathbf{x})\partial_t^2 v_z(\mathbf{x},t) - \partial_z [\lambda(\mathbf{x})(\partial_x v_x(\mathbf{x},t) + \partial_z v_z(\mathbf{x},t)) + 2\mu(\mathbf{x})\partial_z v_z(\mathbf{x},t)] \\ + \partial_x [\mu(\mathbf{x})(\partial_x v_z + \partial_z v_x)] = F_z(\mathbf{x},t), \end{aligned} \quad (7)$$

where,

$$F_x(\mathbf{x},t) = \partial_t f_x(\mathbf{x},t) - \partial_t [\partial_x I_{xx}(\mathbf{x},t) + \partial_z I_{xz}(\mathbf{x},t)], \quad (8)$$

$$F_z(\mathbf{x},t) = \partial_t f_z(\mathbf{x},t) - \partial_t [\partial_x I_{xz}(\mathbf{x},t) + \partial_z I_{zz}(\mathbf{x},t)]. \quad (9)$$

Note that similar set of second-order differential equations can be derived for the stress field. In practice, we need only to solve for one of the two sets.

For the staggered grid implementation we can use equations (1)-(5) to model seismic wave propagation.

In order to solve either equations (1)-(5) or (6)-(9), it is essential to set the boundary and initial condition for the problem of modeling wave propagation through the subsurface. The initial conditions for the particle velocity and the stress fields and their time derivatives are null before the firing of seismic source.

$$\begin{aligned} \mathbf{v} = \partial_t \mathbf{v} = \mathbf{0}, \quad t \leq 0, \\ \boldsymbol{\tau} = \partial_t \boldsymbol{\tau} = \mathbf{0}, \quad t \leq 0. \end{aligned} \quad (10)$$

The boundary conditions for the problem of modeling seismic wave propagation are

determined by the free surface: air-solid in the case of land seismic and air-water in the case of marine seismic. Let us assume the free surface to be  $z = 0$ . Then the boundary condition is

$$\tau_{zz}(x, z = 0, t) = \tau_{xz}(x, z = 0, t) = 0 \quad (11)$$

or equivalently

$$\begin{aligned} & [\lambda(\mathbf{x}) + \mu(\mathbf{x})] \partial_z v_z(x, z = 0, t) + \lambda(\mathbf{x}) \partial_z v_z(x, z = 0, t) \\ & = \mu(\mathbf{x}) [\partial_z v_x(x, z = 0, t) + \partial_x v_z(x, z = 0, t)] = 0. \end{aligned} \quad (12)$$

The rest of the medium is unbounded.

### Discretization in both Time and Space

We discretize both the time and space domain as follows

$$\begin{aligned} t &= n\Delta t, \quad n = 0, 1, 2, \dots, N, \\ x &= i\Delta x, \quad i = 0, 1, 2, \dots, I, \\ z &= k\Delta z, \quad k = 0, 1, 2, \dots, K. \end{aligned} \quad (13)$$

This discretization is called the reference grid. For the case of staggered grid technique, which was used in the FDM codes to generate synthetic data for our various investigations, not all quantities in the differential equations (1)-(5) are grid at the point of reference grid. Some quantities are defined as  $x = \left(i \pm \frac{1}{2}\right) \Delta x$  instead of  $x = i\Delta x$ .

Figure 1 shows an example of staggered gridding of the quantities entering in the equations 1-5. Note that the Normal stresses, mass density, and Lamé parameters are defined at the points on the reference grid, whereas the shear stresses and the three

components of the particle velocity are defined as the points half a grid off the reference grid.

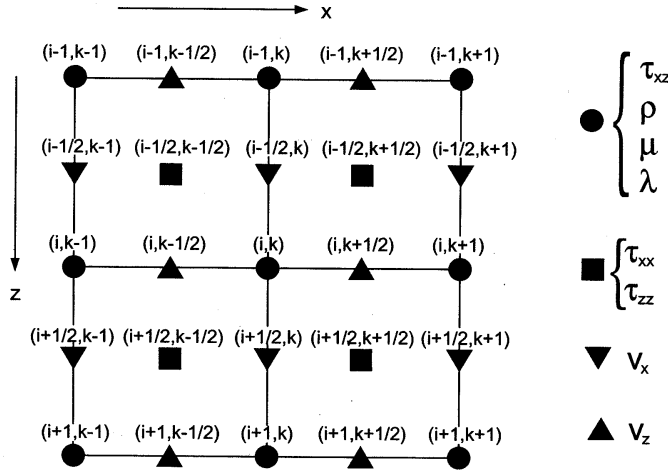


Figure 1: An illustration of the staggered grid technique (Ikelle and Amundsen, 2003)

### Staggered Grid Implementation

The discrete form of equations (1)-(5) is given as

for particle velocity

$$[v_x]_{i+1/2,k}^{n+1/2} = [v_x]_{i+1/2,k}^{n-1/2} + [\Delta t b_x (D_x \tau_{xx} + D_z \tau_{xz} + F_x)]_{i+1/2,k}^n \quad (14)$$

$$[v_z]_{i+1/2,k}^{n+1/2} = [v_z]_{i+1/2,k}^{n-1/2} + [\Delta t b_z (D_x \tau_{xz} + D_z \tau_{zz} + F_z)]_{i+1/2,k}^n \quad (15)$$

and for stresses,

$$[\tau_{xx}]_{i,k}^{n+1} = [\tau_{xx}]_{i,k}^n + \Delta t [(\lambda + \mu) D_x v_x + D_z v_z]_{i,k}^{n+1/2} \quad (16)$$

$$[\tau_{zz}]_{i,k}^{n+1} = [\tau_{zz}]_{i,k}^n + \Delta t [(\lambda + \mu) D_z v_z + D_x v_x]_{i,k}^{n+1/2} \quad (17)$$

$$[\tau_{xz}]_{i+1/2,k+1/2}^{n+1} = [\tau_{xz}]_{i+1/2,k+1/2}^n + \Delta t [\mu_{xz} (D_z v_x + D_x v_z)]_{i+1/2,k+1/2}^{n+1/2} \quad (18)$$

with

$$b_x = \frac{1}{2} [b_{1,k} + b_{i+1,k}] \quad (19)$$

$$b_z = \frac{1}{2} [b_{1,k} + b_{i+1,k}] \quad (20)$$

$$\mu_{xz} = 4 \left[ \frac{1}{\mu_{i,k}} + \frac{1}{\mu_{i+1,k}} + \frac{1}{\mu_{i,k+1}} + \frac{1}{\mu_{i+1,k+1}} \right]^{-1} \quad (21)$$

where  $b_x$  and  $b_z$  are the effective medium parameters for the reciprocal of density,  $\mu_{xz}$  is effective medium parameter for rigidity. The operator  $D_x, D_z$  denote the first-order derivative of  $x$  and  $z$  respectively. Note that the operators are generally evaluated by either a second-order difference or a fourth order difference. For this thesis we use the fourth-order difference.

$$D_x g_{i,j,k} \approx \frac{1}{\Delta x} \left[ \frac{9}{8} (g_{i+1/2,k} - g_{i-1/2,k}) + \frac{1}{24} (g_{i+1/2,k} - g_{i-1/2,k}) \right] \quad (22)$$

### Boundary Conditions

For this thesis, the free-surface condition given in equation (10) is that the normal stress, and the shear stress are null at  $z=0$ . The horizontal spatial derivative is no problem in staggered grid implementation in equations (14)-(18). However the vertical spatial derivative, we have to add two grid points above  $z = 0$ .

$$[\tau_{xz}]_{i,k=0}^{n+1} = 0, [\tau_{xz}]_{i,k=-1}^{n+1} = -[\tau_{xz}]_{i,k=1}^{n+1} \quad (23)$$

$$[\tau_{zz}]_{i+1/2,k=-1/2}^{n+1} = -[\tau_{zz}]_{i+1/2,k=1/2}^{n+1} \quad (24)$$

$$[\tau_{zz}]_{i+1/2,k=-3/2}^{n+1} = -[\tau_{zz}]_{i+1/2,k=3/2}^{n+1} \quad (25)$$

The rest of the medium is considered to be absorbing boundary. This condition is obtained by multiplying the stress and particle velocity by the factor,

$$G(i) = \exp\left\{-\left[\frac{0.3}{i \max}(i \max - i)\right]\right\}, \text{ for } 1 \leq i \leq i \max \quad (26)$$

$i \max$  is the strip width in number of grid points.

### Limitations

The stability problems that can be experienced in the explicit method can be due to recursive computation and timestep by timestep. Note that the instability can occur if the ratio between the temporal and spatial sampling intervals is not constrained as

$$\Delta t < 0.606 \frac{\Delta x}{V_{\max}}$$

where  $V_{\max}$  is the maximum velocity in the 2D geological model.

Another type of instability can be due to the grid-dispersion. The condition to avoid the grids dispersion is related to the number of grid points per wavelength.

## VITA

### **Abiola Omobolaji Oladeinde**

Department of Geology and Geophysics

Texas A&M University, College Station, TX 77843-3115

267-218-2934

### **Education**

M.S., August 2005, Texas A&M University, Department of Geology and Geophysics. Thesis: Linear demultiple solution based on bottom multiple generator (BMG) reflector approximation. Major Geophysics.

B.S., September 1997, University of Ibadan, Department of Physics. Research: Performance tests on ion chamber and thermoluminescent dosimeter in radiation dose measurements. Major Physics.

### **Unpublished Publication**

Watts A. O. and Ikelle, L. T., 2005, Linear demultiple solution based on bottom multiple generator (BMG) reflector approximation: some new results.

### **Permanent address**

153 Mike Gartrell Circle, Sacramento, CA 95835 USA

email: abiola25@yahoo.com

(267) 218 2934